Development of magnetic mesoporous silica composites as adsorbents for aqueous pollutants

水質汚染物質の吸着剤としての磁性メソポーラスシリカ複合材料の開発

Puji Lestari

Division of Materials Engineering
Graduate School of Engineering
Gifu University

March 2022

Contents

Chapter 1 Introduction 1

1.1. Background of the research 1

1.2. Objectives of the research 2

1.3. Structure of the thesis 3

1.4. References 3

Chapter 2 Literature review 5

2.1. Synthetic dyes 5

2.2. Adsorption 5

2.3. Porous adsorbents 8

2.4. References 11

Chapter 3 One-pot alkanolamines-assisted synthesis of magnetic mesoporous silica for synthetic dye adsorption 14

3.1. Introduction 14

3.2. Materials and methods 16

3.3. Results and discussion 19

3.4. Conclusions 31

3.5. References 31

Chapter 4 Microwave-assisted synthesis of magnetic silica-MIL-100(Fe) composite as an adsorbent for dye 35

4.1. Introduction 35

4.2. Materials and methods 37

4.3. Results and discussion 42

4.4. Conclusions 52

4.5. References 53

Chapter 5 Preparation and characterization of magnetic mesoporous silica@MIL-(Fe) composite for the removal of cationic and anionic dyes from water 56

5.1. Introduction 56

5.2. Materials and methods 57

5.3. Results and discussion 59

5.4. Conclusions 64

5.5. References 65

Chapter 6 General conclusions and future perspectives 66

6.1. General conclusions 66

6.2. Future perspectives 67

List of figures 68

List of tables 70

List of publications 71

List of presentations 72

Curriculum vitae 73

Acknowledgement 74

Chapter 1

Introduction

1. 1 Background of the research

Water is a basic requirement for humankind. However, the continuing growth of population and industrialization is followed by the decrease of environmental water quality. The amount of aqueous pollutants disposed into the water bodies also continues to increase overtime, leading to the clean water issues. It is estimated that more than 1.2 billion people of the global population face difficulties in accessing clean and safe drinking water.[1] Therefore, the issues regarding clean water and water pollution are considered one of the most important problems we face today.

Among the water pollutants, dyes are considered one of the top pollutants due to their extensive application in various industries including textile industry, paint, printing, leather, food, plastic, and others. This extensive application has led to the discharged of dyes-containing industrial effluents into the environment, especially into the water bodies.

Although most of the industrial effluents are treated prior to the discharge in order to meet the suitable criteria for the discharged water, the dyes residue in the effluent still possess a potential threat for the aquatic environment. The dye residues, even at a very low concentration (< 1 ppm) may cause an aesthetic problem due to the unwanted change of water color.[2] The change of water color might also reduce the sunlight penetration into the water body, preventing the aquatic plants' photosynthesis. Besides, the synthetic dyes are also known for their carcinogenic and mutagenic properties, making them a potential threat to human health and aquatic life.[3]

Various technologies have been developed to efficiently remove synthetic dyes from wastewater such as chemical oxidation,[4]photocatalytic degradation,[5] adsorption,[6-8] membrane filtration, and coagulation/flocculation.[9,10] Each treatment technology has its own advantages and disadvantages. Among the above-mentioned technologies, adsorption is considered the

most effective due to its efficiency, low-cost process, technical feasibility, reusability and easy operation.[11] Thus, the development of new adsorbents material with fast kinetics and high adsorption capability towards synthetic dyes is crucial.

One of the most promising materials for the adsorption process of synthetic dyes is porous materials. The use of porous materials in the conventional adsorption process, however, requires a time and energy-consuming separation process to separate the used adsorbents from the solution. The separation of the used adsorbents is commonly conducted using filtration or centrifugation method. The combination of these porous materials with magnetic nanoparticles as an adsorbent would provide a more convenient adsorption process. The used adsorbent could be easily separated from the aqueous solution using an external magnetic force, providing a cleaner and fast separation method.[12,13]

In this study, the magnetic composites of porous materials were prepared using more environmentally friendly methods such as one-pot system and microwave irradiation. The prepared composites were then tested for their ability to adsorb synthetic dyes from water.

1. 2 Objectives of the research

The aim of this study is to develop an effective adsorbent based on magnetic mesoporous silica composite for removing organic dyes from water using environmentally friendly methods.

The effectiveness of the composites was investigated by studying thoroughly the characteristics and properties of the composite. In addition, some parameters that influence the adsorption ability of the composites towards the chosen pollutants were also observed. Thus, the objectives of this study are as follows:

- To synthesize and characterize magnetic mesoporous silica composite using one-pot system.
- To synthesize and characterize magnetic mesoporous silica-MIL-100(Fe) composite using microwave assisted method.
- Apply the synthesized composites as adsorbents for synthetic dyes in water.

1.3 Structure of the thesis

This thesis consists of 6 chapters; Chapter 1 introduces the background and objectives of the research. Chapter 2 reviews the literature about synthetic dyes, magnetic mesoporous silica, metal organic frameworks (MOFs), their composites and adsorption process. Chapter 3 studies the synthesis of magnetic mesoporous silica (MMS) using various alkanolamines as basic reagents in a one-pot system. The prepared MMS materials were tested for their adsorption properties for brilliant green dye in water. Chapter 4 conducts the study about the preparation of a magnetic silica-MOF composite under microwave irradiation to effectively remove Congo red dye from the solution. Chapter 5 explains about the synthesis of magnetic mesoporous silica@MIL-100(Fe) and its ability in removing the cationic and anionic dyes from water. The composite in this chapter is synthesized through the conventional hydrothermal method. The last chapter, Chapter 6, concludes the finding of this study and suggests the future works that can be carried out.

1.4 References

1. S. J. Tesh and T. B. Scott,*Adv. Mater.*, **2014**, 26, 6056-6068. https://doi.org/10.1002/adma.201401376

2. M. M. Ayad, A. A. El-Nasr, *J. Phys. Chem.* C, **2010**, 114, 14377-14381. https://doi.org/10.1021/jp103780w

3. D. Rawat, V. Mishra, and R. S. Sharma, *Chemosphere*, **2016**, 155, 591-605. https://doi.org/10.1016/j.chemosphere.2016.04.068

4. X. Z. Xiao, T. T. Dai, J. Guo, and J. H. Wu, *ACS App.l Nano Mater.,* **2019**, 2, 4159-4168. https://doi.org/10.1021/acsanm.9b00638

5. V. A. Tran, K. B. Vu, T. T. Vo, V. T. Le, H. H. Do, L. G. Bach, and S. Lee, *Appl. Surf. Sci.*,**2021**, 538, 148065. https://doi.org/j.apsusc.2020.148065

6. R. Ianoş, C. Păcurariu, S. G. Muntean, E. Muntean, M. A. Nistor, and D. Nižňanský, *J. Alloys Compd.*, **2018**, 741,1235-1246. https://doi.org/10.1016/j.jallcom.2018.01.240

7. I. M. Lipatova, L. I. Makarova, and A. A. Yusova, *Chemosphere,***2018**, 212, 1155-1162. https://doi.org/10.1016/j.chemosphere.2018.08.158

8. G. V. Brião, S. L. Jahn, E. L. Foletto, and G. L. Dotto, *J Colloid Interf. Sci.*,**2017**, 508, 313-322. https://doi.org/10.1016/j.jcis.2017.08.070

9. J. Castañeda-Díaz, T. Pavón-Silva, E. Gutiérrez-Segura, and A. Colín-Cruz, *J. Chem.*,**2017**, 5184590. https://doi.org/10.1155/2017/5184590

10. M. R. Gadekar and M. M. Ahammed, *Desalin. Water Treat*.,**2016**, 57, 26392-26400. https://doi.org/10.1080/19443993.2016.1165150

11. Y. Zhou, L. Yu, Y. Gao, J. Wu, and W. Dai, *Ind. Eng. Chem.Res*.,**2019**, 58, 19202-19210. https://doi.org/10.1021/acs.iecr.9b03815

12. S. Egodawatte, A. Datt, E. A. Burns, and S. C. Larsen, *Langmuir*, **2015**,31, 7553-7562. https://doi.org/10.1021/acs.langmuir.5b01483.

13. R. K. Sharma, M. Yadav, and M. B. Gawande, *ACS Symp. Ser. Am. Chem. Soc*., **2016**, 1238, 1-38. https://doi.org/10.1021/bk-2016-1238.ch001.

Chapter 2

Literature Review

2.1 Synthetic dyes

Dyes are colored organic compounds that are applied to add color to various materials in paper, paint, leather, cosmetics, plastic, textile, rubber, and other industries. Dyes are mainly classified into natural and synthetic dyes. In the industrial applications, the synthetic dyes are mainly used due to their stability, inertness to biodegradation, a wide range of color and intensity, easy application, and low cost.[1,2] Dyes mainly contain two types of groups which are responsible for their color, one is the *chromophore* and the other is the *auxochromes*. Chrompohores are groups that are responsible for dyeing the materials, such as O=(C_6H_4)=O, -C=O, -N=N-, and –NO_2. While auxochromes are defined as the groups that increase the fiber affinity for color and decrease the water-solubility by donating or withdrawing electrons, such as –SO_3H, -NH_3, -OH and -COOH.[3] Based on their solubility, dyes can be classified into water-soluble such as acid, basic, reactive and direct dye, and water-insoluble dyes such as vat, disperse and sulfur dyes.[4]

When released into the environment, synthetic dye materials cause not only harmful effects but also aesthetic problems in water. The small concentration of dyes could give an unwanted color to the water and reduce the oxygen levels and light availability in the aquatic environment. The presence of dyes in aquatic environment will further affect the development rate and inhibits the growth of aquatic plants.[5] Many recent studies have reported the presence of synthetic dyes in various aquatic environments including groundwater, soil and surface water due to their extensive application in industries.[6]

2.2 Adsorption

Adsorption is the attachment of molecules from the gaseous or liquid phase to the condensed layer on a solid surface, as illustrated in **Fig.2-1**. The solid material which provides

the surface for adsorption process is called the *adsorbent* while the *adsorbate* is the molecules that are adsorbed to the surface of the adsorbent. The adsorbed particle could be released from the surface of the adsorbent, this process is called desorption.

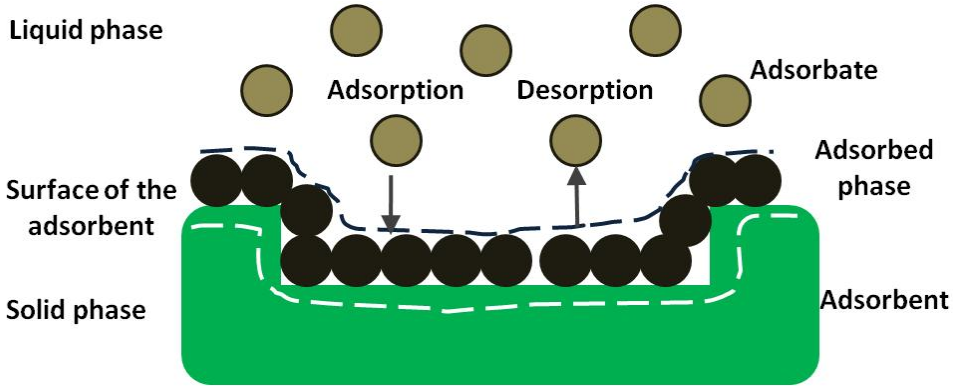

Fig.2-1. Adsorption process

In the adsorption process, the surface of the adsorbent plays a crucial role. The engineered adsorbents are mostly porous materials having the surface area between 100 – 1000 $m^2 g^{-1}$.[7]

Adsorption process could be divided into two types; chemical adsorption (chemisorption) and physical adsorption (physisorption). In chemisorption, there is a direct chemical bond between the adsorbate and one or more atoms on the surface of adsorbent, while in physisorption, there is no direct bond between the adsorbate and the surface of the adsorbent. The adsorbate is held by physical (i.e., van der Waals) forces instead.

2.2.1 Adsorption isotherms

Adsorption isotherm is a function that correlates the amount of adsorbate on the adsorbent, with its pressure (gas) or concentration (liquid). Many adsorption isotherm models have been developed to describe the adsorption process. Among those models, Langmuir and Freundlich isotherm models are the most commonly used due to their simplicity.

Langmuir isotherm model is the simplest physically plausible isotherm based on the assumptions that the adsorption cannot proceed beyond monolayer coverage and there are no interactions between the adsorbed molecules.[8] Langmuir isotherm can be expressed by the following equation:

$$q_e = q_{max}\frac{K_L C_e}{1 + K_L C_e}$$

The parameter C_e is the concentration of adsorbate remained in the solution, q_e is the equilibrium amount of adsorbate loaded on the adsorbent, q_{max} is the maximum adsorption capacity of the adsorbent, and K_L is Langmuir constant. The q_{max} and K_L are temperature dependent parameters.

The Langmuir isotherm is designed for monolayer adsorption of a species on a homogenous surface, while the Freundlich isotherm is for multilayer adsorption on a heterogeneous surface. The mathematical equation for Freundlich model is as follows:

$$q_e = K_f C_e^{\frac{1}{n}}$$

The parameter K_F is the constant related to Freundlich adsorption capacity and n is a parameter that represents the heterogeneity of the system.

2.2.2 Adsorption kinetics

In the adsorption process, kinetic performance of an adsorbent is also of a great importance. Kinetics describes the rate at which the adsorption process occurs. Adsorption kinetics in liquid phase depends on many factors such as the size and the molecular structure of the adsorbate, properties of the solvent, and properties of the adsorbent. In order to study the mechanism of adsorption and potential rate controlling steps, some kinetic models have been applied to test the data from experiment. The most widely used kinetic models for adsorption process are pseudo-first order kinetic model and pseudo-second order kinetic model. The pseudo-first order is described by the following equation:[9]

$$\ln\left(\frac{q_e}{q_e - q_t}\right) = k_1 t$$

The pseudo-second order kinetic model is expressed by a linear equation as follows:[10]

$$\frac{t}{q_t} = \frac{1}{k_2 q_e^2} + \frac{t}{q_e}$$

The parameters q_e and q_t (mg g^{-1}) represent the adsorption capacity at equilibrium and at time t (min), respectively. The parameters k_1 (L min^{-1}) and k_2 (g mg^{-1} min^{-1}) are the rate constant of pseudo-first order kinetics and pseudo-second order kinetics, respectively. If the pseudo-second order model is applicable for an adsorption process, the plot of *t/qt* versus *t* should give a linear relationship. The values of q_e, and *k* could be determined from the slope and intercept of the linear graph, respectively.

2.3 Porous adsorbents

Porous materials are materials that have pores on their structure, causing the material to have an internal surface area. According to the recommendation from IUPAC (1985), the pores of the porous materials are classified based on their size:[11]

(i) pores with widths larger than 50 nm are called *macropores*;

(ii) pores with widths between 2 – 50 nm are called *mesopores*;

(iii) pores with widths smaller than 2 nm are called *micropores*.

The internal structure of the pores (interconnected and non-interconnected) will dictate the properties of the materials such as reactivity, thermal conductivity as well as the kinetics of various transport processes. Mesoporous silica and metal organic frameworks are among the most studied porous materials for application as adsorbents.

2.3.1 Mesoporous silica

Mesoporous materials are defined as materials having the pore size in the range 2-50 nm. The pore size of the mesoporous materials is dependent on the choice of the surfactants used in the synthesis. The synthesis of ordered mesoporous silica (MCM-41) was first reported by Mobil Company in 1992. The method is based on the condensation of silica precursors in the

presence of cationic surfactants cetyltrimethylammonium bromide (CTAB) as a structure-directing agent under hydrothermal and basic conditions.[12] The possible mechanism of mesostructure formation in MCM-41 is illustrated in **Fig. 2-2**. Mechanism 1 is regarded as the true liquid-crystal templating mechanism in which the surfactants form a liquid-crystal phase prior to the precipitation.[13] Mechanism 2 is the cooperative liquid-crystal mechanism with no distinct liquid-crystal phase or also known as cooperative surfactants/inorganic self-assembly.[14]

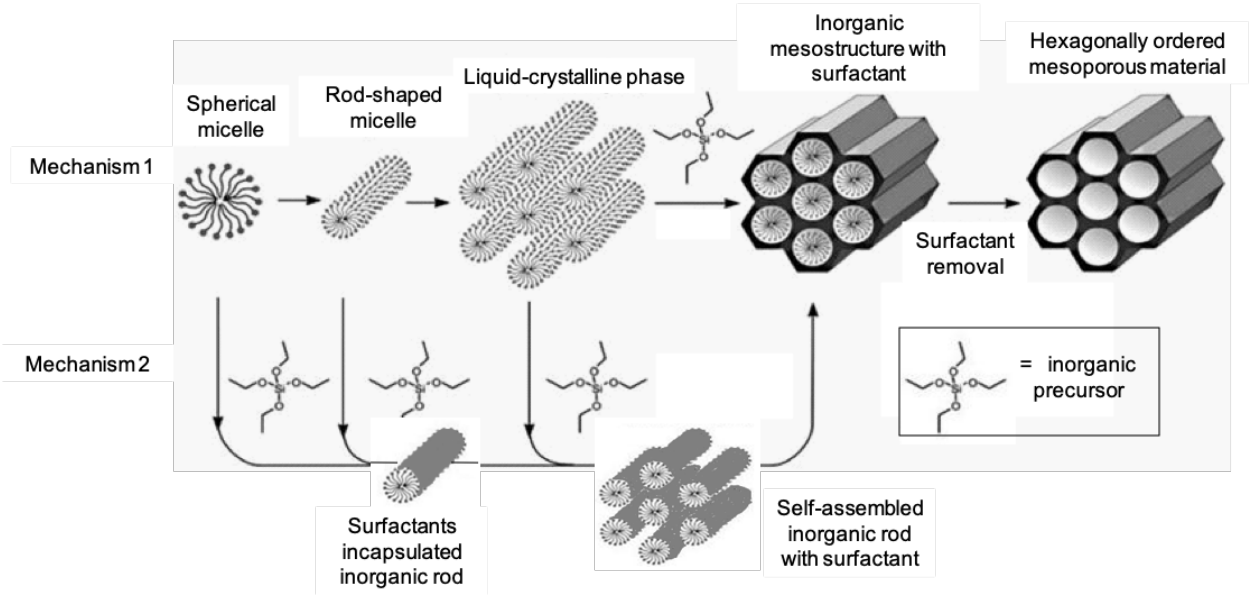

Fig. 2-2. Possible mechanism of mesostructure formation in MCM-41.[15]

Besides MCM-41, various mesoporous silica materials have been synthesized by varying the precursor materials and reaction conditions. Mesoporous silica is amorphous material that exhibits a high degree of pore order, high thermal stability, narrow pore size distribution, and high surface area (up to 1000 $m^2 g^{-1}$). Due to its properties, mesoporous silica has been widely used in the adsorption of heavy metals, organic dyes, and other organic pollutants in water.[16]

2.3.2 Metal organic frameworks (MOFs)

Metal organic frameworks (MOFs) are crystalline, porous frameworks which self-assemble to form coordination bonding between transition metal cations and organic linkers/ligands.[17]The examples of the organic ligands in MOFs structure are terephthalate, imidazolate, sulphonate,

amines, carboxylate, and others.[18] A schematic representation of the synthesis of MIL-100(Fe), a type of MOFs, is given in **Fig. 2-3**. The presence of these organic ligands provides more functionality for the adsorption of various organic and inorganic molecules through one or more interaction mechanism such as van der Waals interaction, $\pi - \pi$ interaction, dipole-dipole, chelation, hydrophobic interaction, hydrogen bonding, etc.[19]

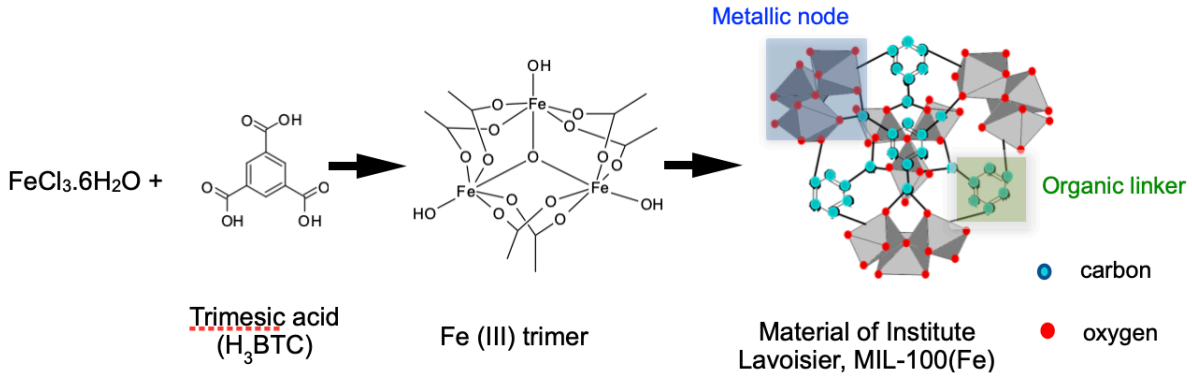

Fig. 2-3. Schematic representation of the synthesis of MIL-100(Fe).

Other superior characteristics of MOFs which support their application in adsorption process include high specific surface area, surface functionality, and uniform porosity.[20]The surface area, pore size, and shape of MOFs can be tuned easily by tuning the synthesis' parametes.[21] Due to their excellent properties, MOFs have become one of the most widely studied porous material for wastewater treatment.[22]

Several types of MOFs are university of Oslo (UiO), zeoliticimmidazolate frameworks (ZIF), material Institute Lavoiser (MIL), isoreticular-based MOFs, and others. Among these MOFs, MIL-based MOFs shows an excellent stability in aqueous solution, making them potential for adsorption process in aqueous system.[23]

2.3.3. Magnetic composite

Magnetic composite materials are materials consist of a base material that is embedded with magnetic nanoparticles which are oxides of metals, most commonly iron (Fe).[24] The synthesis of adsorbent particles with magnetic properties and high adsorption ability offers a

new tool for water purification.[25] Many studies have been reported about the ability of magnetic composite for adsorption of pollutants, especially synthetic dyes, from water.[26] Magnetic composite materials offers an additional advantages for the separation of the used adsorbent using an external magnetic force.[27] In addition, magnetic composite materials may exhibit synergistic effect of the combination of the host and guest compounds which can enhance the adsorption capability.[28]

Although many studies have been reported on the application of magnetic composite for adsorption purpose with high adsorption capacity, rapid adsorption kinetics, good selectivity and recyclability, most of the studies are still on the laboratory scale.[29] The limitations for the scale-up applications of magnetic composite adsorbents are related to the mechanical stability, chemical stability, optimization of the synthesis, toxicity levels, regeneration, and reusability.[30]

2.4 References

1. P. Zucca, G. Cocco, F. Sollai, and E. Sanjust, *Biocatalysis*, **2015**, 1, 82-108. https://doi.org/10.1015/boca-2015-0007
2. A. Paz, J. Carballo, M. J. Pérez, and J. M. Domínguez, *Chemosphere*, **2017**, 181, 168-177. https://doi.org/10.1016/j.chemosphere.2017.04.046
3. R. L. M. Allen, *The chemistry of azo dyes. In: Colour Chemistry.* Studies in Modern Chemistry,Springer, Boston, **1971**.
4. M. Berradi, R. Hsissou, M. Khudhair, M. Assouag, O. Cherkaoui, A. El Bachiri, and A. El Harfi, *Heliyon*, **2019**, 5. http://doi.org/10.1016/j.heliyon.2019.e02711
5. J. Sharma, S. Sharma, and V. Soni, *Reg. Stud. Mar. Sci.*, **2021**, 45, 101802. https://doi.org/10.1016/j.rsma.2021.101802
6. D. Ghosh and K. G. Bhattacharyya, *Appl. Clay Sci.*, **2002**, 20, 295-300. https://doi.org/10.1016/S0169-1317(01)00081-3
7. I. Ali, *Chem. Rev.,* **2012**, 112, 5073-5091. https://doi.org/10.1021/cr300133d

8. P. W. Atkins and J. de Paula, *Atkins' Physical Chemistry (6th ed.)*, Oxford University Press, Oxford, **2006**.
9. Y. S. Ho, *Scientometrics,* **2004**, 59, 171-177. https://doi.org/10.1023/B:SCIE.0000013305.99473.cf
10. Y. S. Ho and G. McKay, *Trans IChemE*, **1998**, 76, 332-339. https://doi.org/10.1205/09578298529696
11. K. S. W. Sing, D. H. Everett, R. A. V. Haul, L. Moscou, R. A. Pierotti, J. Rouquerol, and T. Siemieniewska, *Pure Appl. Chem.*, **1985**, 57, 603-619. https://doi.org/10.1351/pac198557040603
12. J. L. Vivero-Escoto, B. G. Trewyn, and V. S. Y. Lin, *Annu. Rev. Nano Res.*, **2010**, 3, 191-231.
13. G. S. Attard, J. C. Glyde, and C. G. Göltner, C. G., *Nature*, **1995**, 378, 366-368. https://doi.org/10.1038/37836610
14. F. Schüth, *Chem. Mater.*, **2001**, 13, 3184-3195. https://doi.org/10.1021/cm011030j
15. P. van der Voort, K. Leus, and E. De Canck, *Introduction to Porous Materials*, Wiley, Singapore, **2019**.
16. R. E. Morsi and R.S. Mohamed, *R. Soc. Open. Sci.*, **2017**,5, 172021. https://doi.org/10.1098/rsos.172021
17. M. Eddaoudi, J. Kim, N. Rosi, D. Vodak, J. Wachter, M. O'Keeffe, and O. M. Yaghi, *Science*, **2002**, 295, 469-472. https://doi.org/10.1126/science.1067208
18. E. E. Moushi, T. C. Stamatatos, W. Wernsdorfer, V. Nastopoulos, G. Christou, and A. J. Tasiopoulos, *Angew. Chem. Int.*, **2006**, 45, 7722-7725. https://doi.org/10.1002/anie.200603498
19. Z. Hasan and S. H. Jhung, J. Hazard. Mater, 2015, 283, 329-339. https://doi.org/10.1016/j.jhazmat.2014.09.046
20. D. Farrusseng, *Metal-Organic Frameworks Applications From Catalysis to Gas Storage*, Wiley-VCH, Weinheim, **2011**.

21. K. A. S. Usman, J. W. Maina, S. Seyedin, M. T. Conato, L. M. Payawan Jr. L. F. Dumée, and J. M. Razal, *NPG Asia Mater.*, **2020**, 12, 58. https://doi.org/10.1038/s41427-020-00240-5
22. D. J. Tranchemontagne, J. R. Hunt, and O. M. Yaghi, *Tetrahedron*, **2008**, 64, 8553-8557. https://doi.org/10.1016/j.tet.2008.06.036
23. X. Qian, B. Yadian, R. Wu, Y. Long, K. Zhou, B. Zhu, and Y. Huang, *Int. J. Hydrog. Energy*, **2013**, 38, 16710-16715. https://doi.org/10.1016/j.ijhydene.2013.07.054
24. O. Philippova, A. Barabanova, V. Molchanov, and A. Khokhlov, *Eur. Polym. J.*, **2011**, 542-559. https://doi.org/10.1016/j.eurpolymj.2010.11.006
25. X. Qu, J. J. Pedro, and A. Qilin Li, *Water Res.*, **2013**, 47, 3931-3946. https://doi.org/10.1016/j.watres.2012.09.058
26. R. Sivashankar, A. B. Sathya, K. Vasantharaj, and V. Sivasubramanian, Environ. *Nanotechnol. Monit. Manag.*,**2014**,1-2, 36-49. https://doi.org/10.1016/j.enmm.2014.06.001
27. K. Manna, and S. K. Srivastava, *ACS Sustain. Chem. Eng.*, **2017**, 5, 10710-10721. https://doi.org/10.1021/acssuschememng.7b02682
28. H. Wang, Y. Xu, L. Jing, S. Huang, Y. Zhao, M. He, H. Xu, and H. Li, *J. Alloy. Compd*., **2017**, 710, 510-518. https://doi.org/10.1016/j.jallcom.2017.03.144
29. A. Mudhoo and M. Sillanpää, *Environ. Chem. Lett*., **2021**, 1-21.https://doi.org/10.1007/s10311-021-01289-6
30. J. You, L. Wang, Y. Zhao, and W. Bao, *J. Clean. Prod*., **2021**, 281, 124668. https://doi.org/10.1016/j.jclepro.2020.124668

Chapter 3

One-pot alkanolamines-assisted synthesis of magnetic mesoporous silica for synthetic dye adsorption

Abstract

Magnetic mesoporous silica (MMS) composites have been synthesized in one-pot system using various alkanolamines (triethanolamine, diethanolamine, tris (hydroxymethyl)aminomethane) as a basic catalyst. The characterization of the composites was conducted using SEM-EDX, TEM, XRD, BET, and XPS instruments. The results revealed that the use of different alkanolamine affected the properties of MMS, including specific surface area, pore volume, and average pore diameter. The MMS synthesized with tris(hydroxymethyl)aminomethane (MMS_{TRIS}) showed the highest specific surface area, pore volume, and average pore diameter among all composites. However, when the composites were applied as adsorbents for brilliant green dye (BG), MMS synthesized with diethanolamine (MMS_{DEA}) showed the highest maximum adsorption capacity of 339.7 mg g^{-1}. The fastest adsorption rate constant of $1.57x10^{-2}$ g mg^{-1} min^{-1} was obtained for MMS_{TRIS}, which has the largest average pore size among all composites. The adsorption kinetic study suggested that the adsorption of BG onto the prepared MMS composites was mainly chemisorption process, which most likely involves electrochemical interaction and hydrogen bonding between BG molecule and the surface of the composites.

Keywords: magnetic mesoporous silica, alkanolamines, one-pot synthesis, dyes adsorption.

3.1 Introduction

Synthetic dyes have been extensively used for the dyeing process in various industries due to their low-cost and easy production, wide spectrum of color, and stability of the color.[1] During the dyeing process, some parts of dyes are lost and discharged as wastewater effluent. The amount of this loss depends on the dye used and the type of dyed materials. Globally,

approximately 700,000 metric tons of 100,000 commercial dyes are produced and up to 70,000 metric tons of these dyes are discharged into wastewater.[2] Most of the wastewater is previously treated to meet the suitable criteria for the discharge water. However, the dye residues in wastewater are still posing potential threats to the aquatic environment. The presence of dye in surface water, even in a very low concentration, may cause aesthetic problems due to the change of water color. Furthermore, the light penetration into the water will be inhibited, preventing the aquatic plant photosynthesis and eventually reducing the oxygen production in water.

Various treatment technologies such as coagulation, chemical oxidation, biodegradation, membrane filtration, adsorption, photocatalysis, and others have been applied for removing dyes from wastewater.[3-8] Each technology has its advantages and limitations. Among those technologies, adsorption is still considered the most effective method due to its simplicity, inexpensive method, and effectiveness.[9-10] Thus, an effort in developing effective adsorbents is a continuing process.

Mesoporous silica, amorphous silica materials with pore size ranging from 2-50 nm, is considered one of the best candidates as an effective adsorbent for dye since it poses many remarkable properties such as high specific surface area, good stability, chemical inertness, as well as porous and tunable structure.[11,12] However, the use of mesoporous silica as an adsorbent requires a further separation process such as filtration and centrifugation to separate the used adsorbent from the treated solution.

The incorporation of magnetic iron oxide nanoparticles on the mesoporous silica material has been attracting much attention recently. The magnetic iron nanoparticles immobilized on mesoporous silica is expected to create a synergistic effect on removing pollutants from aqueous solution by combining the best properties of both materials.[13]Besides, the presence of magnetic nanoparticles on the mesoporous silica will eliminate the filtration or centrifugation process needed after the adsorption process. The used adsorbent could be easily separated

from the aqueous phase using an external magnetic force, providing a cleaner and fast method.[14,15]

Magnetic mesoporous silica (MMS) is frequently synthesized using two steps; magnetic iron nanoparticle synthesis followed by surface modification of the nanoparticles. In this study, MMS was synthesized in one-pot system using various alkanolamine compounds as a basic catalyst. The addition of various alkanolamine compounds is expected to affect the MMS properties since the properties of mesoporous silica are dictated by many factors, including the choice of reagents. The use of one-pot system is preferred since it eliminates the multi-step process and reduces the chemical waste and synthesis time. The efficiency of MMS composites in this work as an adsorbent then was evaluated using brilliant green (BG, **Fig. 3-1**) as a synthetic dye model pollutant.

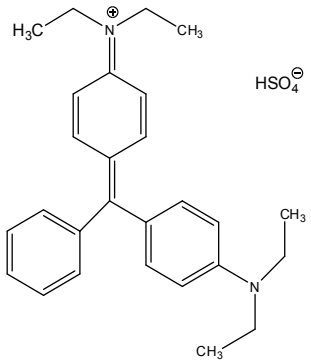

Fig.3-1. Molecular structure of brilliant green dye.

3.2 Materials and methods

3.2.1 Materials

All the chemicals used in the experiments were of analytical grade and were used as received. Cetyltrimethylammonium chloride (CTAC), triethanolamine (TEA), diethanolamine (DEA), ferric chloride hexahydrate ($FeCl_3.6H_2O$) and ferrous chloride tetrahydrate ($FeCl_2.4H_2O$) were purchased from FUJIFILM Wako Pure Chemicals Corporation (Osaka, Japan). Tris(hydroxymethyl)aminomethane (TRIS), 28% ammonia and brilliant green (BG) were obtained from NacalaiTesque, INC (Kyoto, Japan). Tetraethyl orthosilicate (TEOS) was obtained

from Tokyo Chemical Industry Co., Ltd. (Tokyo, Japan). Deionized water (DI) was used to prepare all the solutions.

3.2.2 Synthesis of magnetic mesoporous silica (MMS)

The fabrication of MMS composites was carried out by using cetyltrimethylammonium CTAC surfactant as a template and alkanolamine as a basic catalyst in one-pot system. The synthesis procedure was illustrated in **Fig. 3-2**. MMS was prepared using the following procedure: One hundred milliliter of H_2O was purged with nitrogen gas for 30 min and 410 mg of $FeCl_3.6H_2O$ and 232.6 mg of $FeCl_2.4H_2O$ were dissolved into it. After all of the powders have dissolved, 1 mL of 28% ammonia was added into the solution drop wise and the mixture was stirred for 2 h. After that, 320 mg of CTAC was added and the mixture was stirred for another 10 min. 2.24 mmol of alkanolamine compound (TEA, DEA or TRIS) was added and the mixture was sonicated for 30 min. The molecular structure of each alkanolamine was given in **Fig. 3-3**. The mixture was heated to 80 ^{o}C and was stirred during the heating. During this step, 0.5 mL of TEOS as silica precursor was added into the solution mixture dropwise. The solution was stirred for 3 h afterwards. After the reaction has completed, the products were washed with ethanol and water subsequently. The produced MMS materials were calcined at 500^{o}C for 5 h to remove the templates. The composites synthesized using TEA, DEA and TRIS were called MMS_{TEA}, MMS_{DEA} and MMS_{TRIS}, respectively.

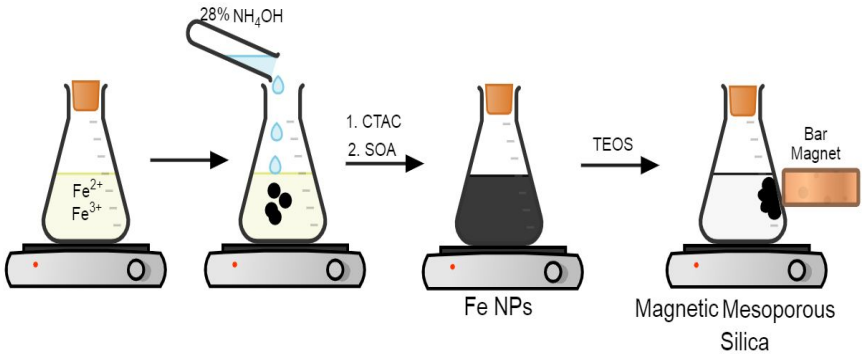

Fig. 3-2. One-pot synthesis of magnetic mesoporous silica.

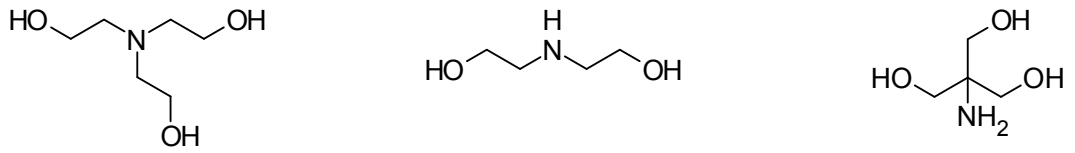

(a) (b) (c)

Fig. 3-3. Molecular structure of alkanolamines: triethanolamine (a); diethanolamine (b); tris(hydroxymethyl)aminomethane (c)

3.2.3 Characterization of MMS

A scanning electron microscope (SEM, Hitachi, S-4300) combined with an EDX (Horiba, EMAX) analyzer was used to capture the surface morphology and to roughly estimate the composition of the materials. The average size and morphology of the materials were observed with a transmission electron microscope (TEM, JEOL, JEM-2100). The specific surface area, total pore volume, and pore size of the materials were determined by N_2 adsorption-desorption isotherm at 77K using a micrometer (Tristar II 3020, Micrometrics). A Fourier-transform infrared spectroscopy (FTIR, Perkin Elmer Spectrum 400) instrument was used to characterize the functional groups present on the materials. The phase structure of the materials was characterized by using an X-ray powder diffraction (XRD, Rigaku Ultima II/PC) instrument with CuK_{α} radiation. The surface chemistry of the materials was analyzed using an X-ray photoelectron spectroscopy (XPS, ULVAC, Quantera XSM) instrument.

3.2.4 Adsorption experiments

Adsorption experiments were carried out in a batch system. Adsorption isotherm of BG onto MMS composites was studied at 25°C with the initial concentration of BG ranging from 10 to 90 mg L^{-1}. A fixed amount of adsorbent was added into BG solution and was stirred for 60 min. Adsorption kinetics of BG onto MMS composites was investigated by mixing 30 mg of adsorbent with 60 mL of 200 mg L^{-1} BG solution. The residual concentration of BG in the mixture was measured at certain time intervals (0-120 min). All adsorption experiments were

conducted in the pH of the original BG solution unless stated otherwise. The adsorption experiment was repeated 3 times and the result was obtained from the average value of the triplicate. The residual concentration of BG in the aqueous solution was measured by using UV-Vis spectrophotometer (Hitachi, U-4100 Spectrophotometer) at a wavelength of 624 nm. The adsorption efficiency and adsorbed amount of dye (q, mg g^{-1}) were calculated using equations 1 and 2:

$$\text{Adsorption efficiency (\%)} = \left(\frac{C_0 - C_t}{C_0} \right) \times 100\% \quad (1)$$

$$q_e = \frac{V\left(C_0 - C_e\right)}{m} \quad (2)$$

where C_0 (mg L^{-1}) is the initial concentration of BG and C_t (mg L^{-1}) is the concentration of BG in aqueous solution at time t; C_e (mg L^{-1}) is the concentration of BG in aqueous solution at equilibrium; V is the volume of solution (L), and m is the adsorbent mass (g).

The recyclability of MMS composites as adsorbents for BG dye was also evaluated by employing acidified ethanol to desorb BG from MMS composites. After sequential washing using distilled water and oven-drying, the adsorbent was reused for adsorption of BG in solution. This adsorption-desorption process was carried out for 4 cycles.

3.3 Results and discussion

3.3.1 Characteristics of MMS

SEM and TEM images of all composites in **Fig. 3.4** showed that all of the MMS composites have a spherical shape and agglomeration were observed in all composites with MMS_{TRIS} showed the less agglomeration. From TEM images, the average particle size of the composites was around 10 nm. The rough estimation of the percentage (w/w) of O, Fe and Si atoms in the composites from EDX measurement showed that MMS_{TEA} gave the highest Fe content among all composites while MMS_{TRIS} showed the lowest Fe content (**Table 3-1**).

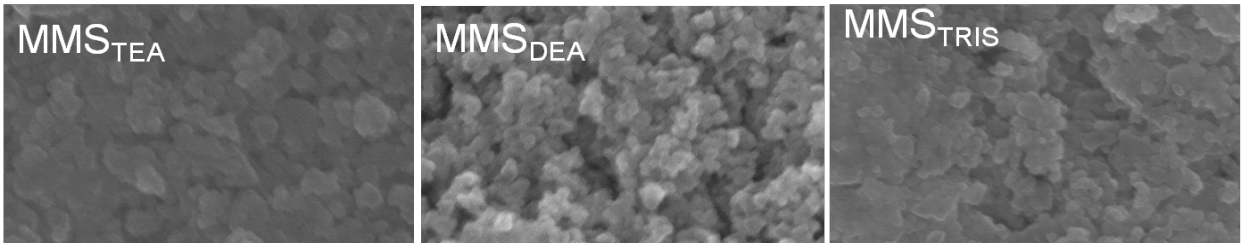

(a)

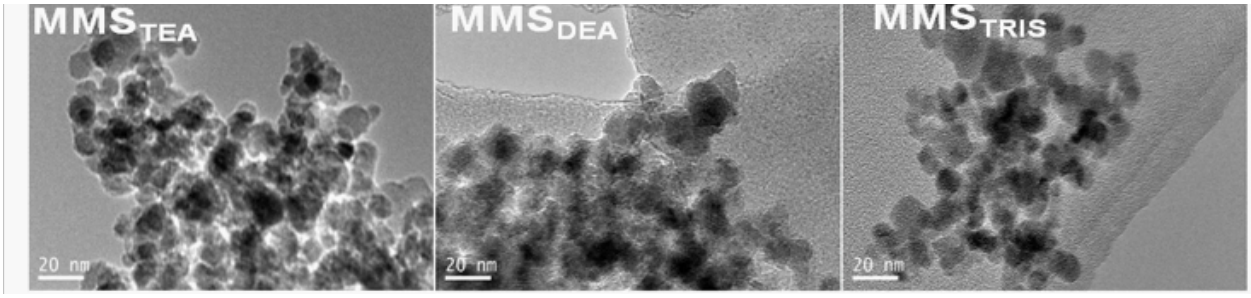

(b)

Fig. 3-4.TEM (a); SEM images and EDX spectra (b) of MMS.

Table 3-1. Result of EDX measurement.

Sample	%O	%Fe	%Si
MMS_{TEA}	68.26	19.35	12.40
MMS_{DEA}	70.55	17.24	12.21
MMS_{TRIS}	71.81	14.36	13.83

The X-Ray diffractogram of all MMS composites was presented in **Fig. 3-5**a. The presences of characteristics peaks at 30°, 35°, 43°, 54°, 57° and 62° were ascribed to (220), (311), (400), (422), (511), and (440) planes of Fe_3O_4, respectively (JCPDS:75-0033), indicating the presence of magnetic iron oxide in all composites. This result showed that the magnetic iron oxide immobilized in silica material maintains its crystalline phase. All composites showed a relatively similar pattern of X-ray diffraction without any obvious peaks of silica material.

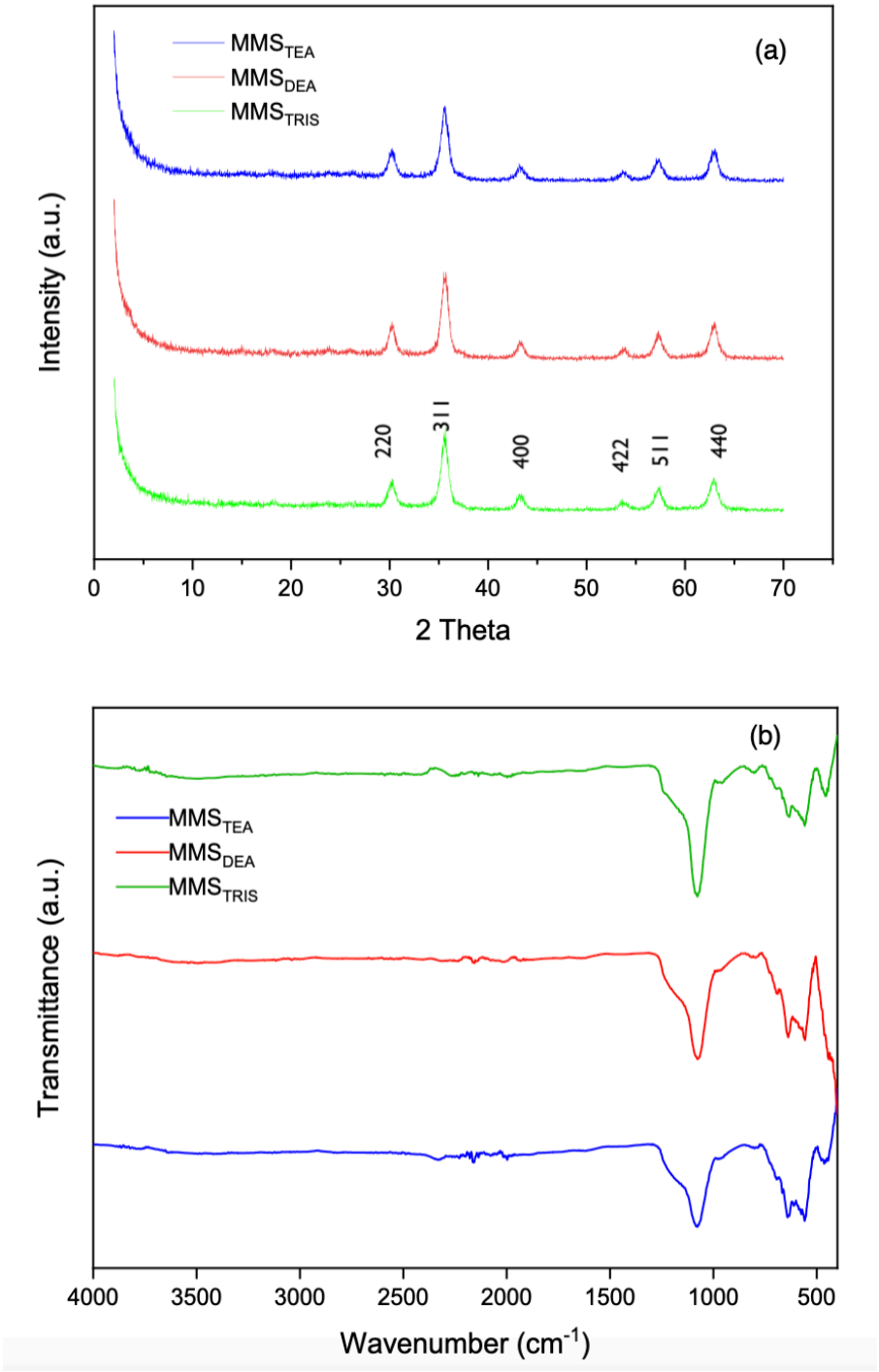

Fig. 3-5. XRD diffractogram (a); FTIR spectra (b); Nitrogen adsorption-desorption isotherm (c) of MMS composites.

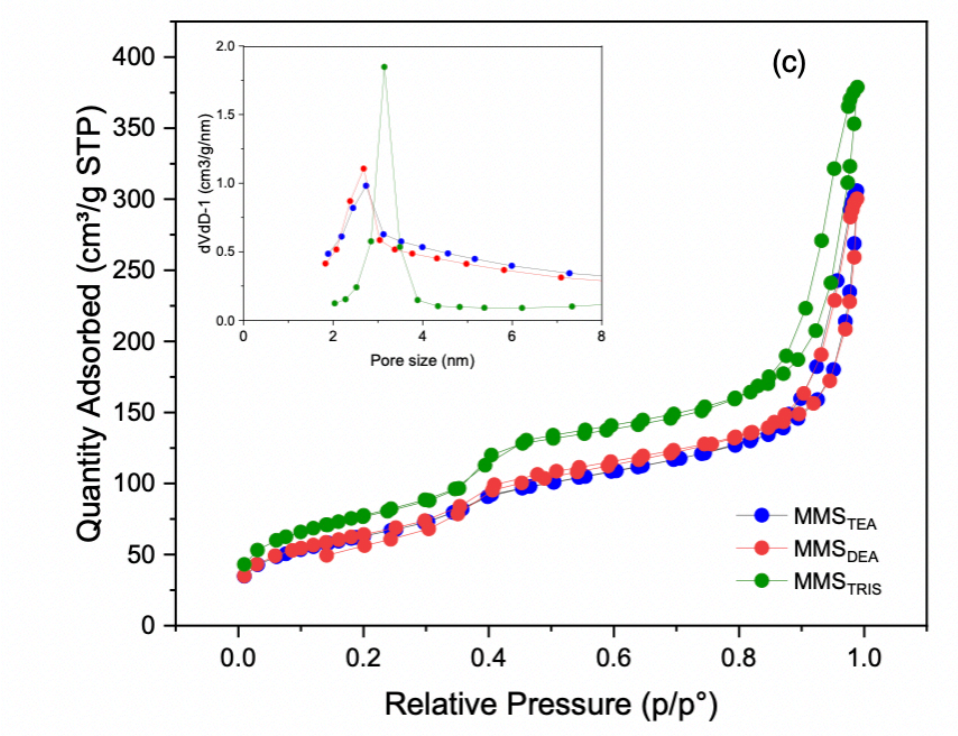

Fig. 3-5.(continuation) XRD diffractogram (a); FTIR spectra (b); Nitrogen adsorption-desorption isotherm (c) of MMS composites.

The FTIR instrument further confirmed the presence of functional groups in the synthesized composites. The FTIR spectra of MMS composites were presented in **Fig. 3-5**b. Each composite showed similar absorbance peak with different intensity, indicating the presence of similar functional groups on the composites. The absorption band at 1090 cm^{-1} was due to the asymmetric stretching vibration of Si-O-Si bonding. The peak at 800 cm^{-1} was attributed to symmetric stretching of Si-O-Si. The appearance of Si-O-Si vibration peaks on the materials indicated that the condensation of silicon alkoxide has occurred.[16] The absorbance peak at 570 cm^{-1} which corresponded to the vibration of Fe-O bonding, also suggested iron oxide's presence on the materials. The FTIR analysis results demonstrated the presence of SiO_2 and Fe_3O_4 in all of the synthesized MMS composites.

The specific surface area and porosity of the composites were determined by liquid N_2 adsorption (at 77 K). The N_2 adsorption-desorption isotherms obtained for the composite

materials were shown in **Fig. 3-5**c. The N_2 adsorption-desorption isotherm curves of all composites exhibited a type IV isotherm and an H1-type hysteresis loop which corresponded to mesoporous materials with a narrow range of mesopores.[17]

Table 3-2. Textural properties of MMS composites.

MMS sample	BET surface area (m^2/g)	Pore volume (cm^3/g)	BJH average pore size (nm)
MMS_{TEA}	228.5	0.416	2.7
MMS_{DEA}	232.0	0.401	2.7
MMS_{TRIS}	280.2	0.546	3.1

Table 3-2 summarized the textural properties of the synthesized MMS. From the BET equation calculation, the specific surface area of each composite was 228.5 m^2/g, 232.0 m^2/g, and 280.2 m^2/g for MMS_{TEA}, MMS_{DEA}, and MMS_{TRIS}, respectively. The surface area of the composites not only depends on the particle size of the material but also the amount of iron nanoparticles immobilized in the materials. The more the iron contents in the composite, the lower the surface area due to the blockage of mesopores by the iron nanoparticles. This data agreed with the EDX data in **Table 3-1**. MMS_{TRIS}, which has the largest specific surface area showed the lowest iron content. All of the synthesized composites showed an average pore size in the range of mesopore size. The MMS_{TEA} and MMS_{DEA} showed relatively similar BET surface area, pore volume, and BJH average pore size while the MMS_{TRIS} showed the highest values among all. These results suggested that the use of alkanolamines with different basicities and structure could influence the properties of the synthesized MMS composites. Alkanolamines could influence the hydrolysis and polycondensation reaction of silica parent material.[16]They could act both as the basic reactant and hydrolysis-retarding agent (complexing agent), which keeps the seeds separated during the condensation process.[18]

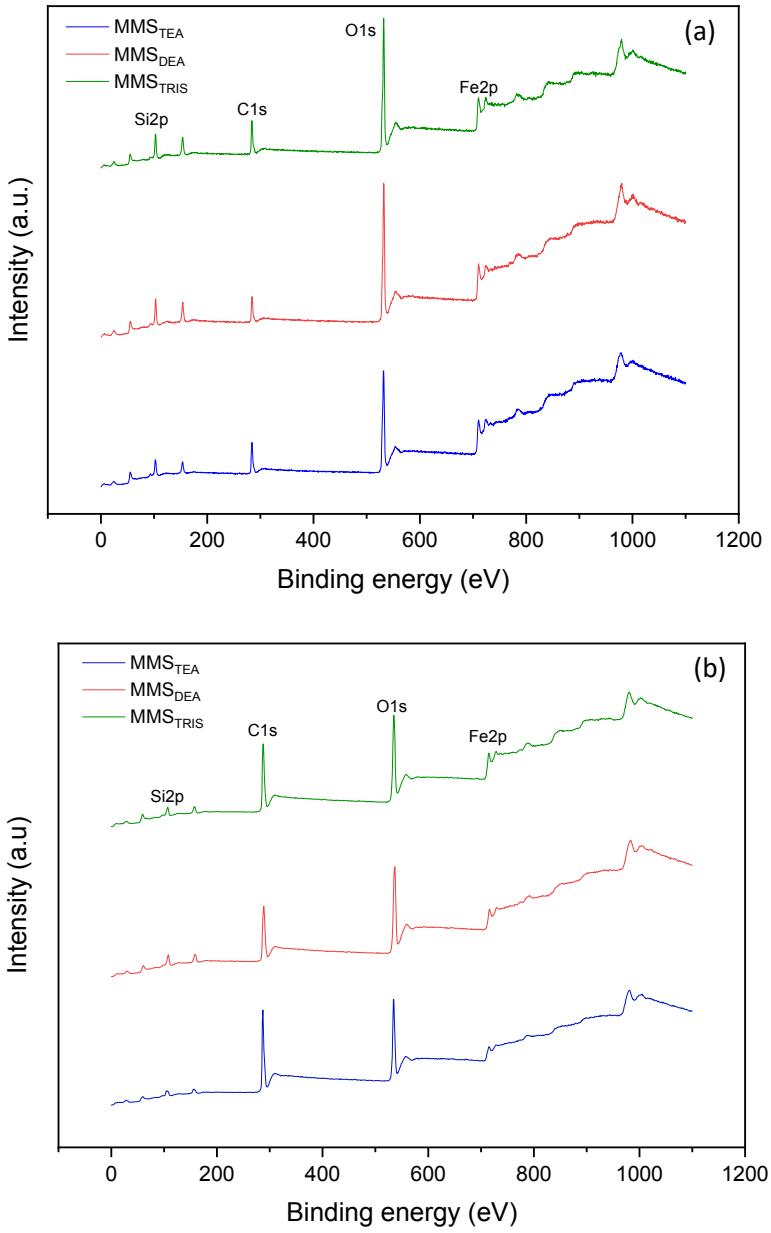

Fig. 3-6. XPS spectra of MMS before (a) and after (b) adsorption of BG.

XPS spectra of MMS composites (**Fig. 3-6**a) showed the peaks of Si, C, O and Fe elements. The binding energies of Fe(III)$2p_{3/2}$ and Fe(III)$2p_{1/2}$ can be seen at 710.5 eV and 724 eV, respectively. This indicated that the iron oxide present in all composites is in the form of magnetite.[19] The presence of silica was shown by Si 2p peak at 102 eV.[20] The XPS spectra of MMS after the adsorption of BG showed a slight increase of the binding energies of Fe(III) in the

iron oxide, as shown in **Fig. 3-6**b. The binding energies of Fe(III)$2p_{3/2}$ and Fe(III)$2p_{1/2}$ were observed at 715 eV and 730 eV, respectively. This increase was due to the decrease of electron density of iron after binding with N^+ of BG molecule.[21]

3.3.2 Adsorption studies

Effect of initial pH

The adsorption performance of the MMS composites was studied using BG as a model pollutant. The effect of solution pH on the adsorption efficiency was studied under the initial solution pH of 3 – 6. At pH lower than 3, BG solution started decolorization while at pH higher than 6, the turbidity and precipitation started to occur. Initial pH of the solution plays an important role in the adsorption efficiency of BG onto MMS composites since the stability and structure of BG molecule and the dissociation of functional groups on the composites are predominantly controlled by solution pH. It was found that the optimum pH of BG adsorption onto all composites was 3, however, since the initial concentration of BG on pH 3 was significantly reduced (**Fig. 3-7**), the adsorption studies were conducted under the original pH of BG solution which was around 4.

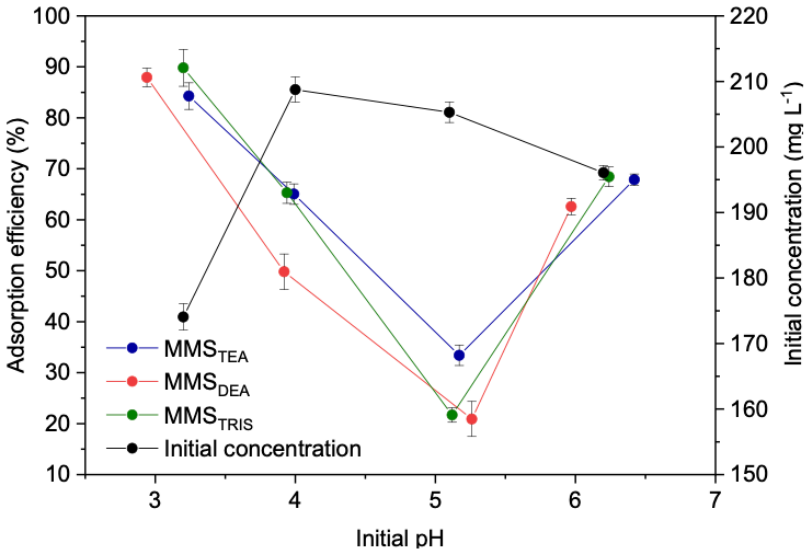

Fig.3-7. Effect of initial pH on adsorption and concentration of BG.

Adsorption kinetics

The adsorption kinetics study provides information about the efficiency of adsorption process. In this work, the kinetic data were evaluated using pseudo-first order and pseudo-second order kinetic models. Pseudo-first order kinetic model is given in Eq. 3.

$$\ln\left(q_e - q_t\right) = \ln q_e - k_1 t \tag{3}$$

While pseudo-second order kinetic model is presented in Eq. 4.

$$\frac{t}{q_t} = \frac{1}{k_2 q_e^2} + \frac{t}{q_e} \tag{4}$$

where t is time (min), q_e and q_t are adsorption capacities at equilibrium and time t, respectively, and k_1 and k_2 are rate constants.

Experiment data were fitted to both kinetic models (**Fig. 3-8**) and all obtained kinetic parameters were given in **Table. 3-3**. It is seen that the adsorption of BG onto all composites followed the pseudo-second order kinetic model with R^2 values greater than 0.99. Moreover, the adsorption capacities obtained from the experiment (q_{exp}) were similar to the values calculated (q_{cal}) from the linear graph equation of pseudo-second order model. This implies that BG's adsorption onto the surface of MMS composites was mainly chemisorption or surface complexation.[22]

Table 3-3.Adsorption kinetic parameters of BG onto MMS composites.

Kinetic model	Parameters	Adsorbent		
		MMS_{TEA}	MMS_{DEA}	MMS_{TRIS}
Experimental	q_{exp} (mg g^{-1})	12.84	14.93	11.50
Pseudo-first order	q_{cal} (mg g^{-1})	10.07	9.05	4.28
	k_1 (min^{-1})	0.016	0.034	0.028
	R^2	0.801	0.874	0.914
Pseudo-second order	q_{cal} (mg g^{-1})	13.51	15.87	11.76
	k_2 (g mg^{-1} min^{-1})	0.0094	0.0073	0.0157
	R^2	0.993	0.991	0.994

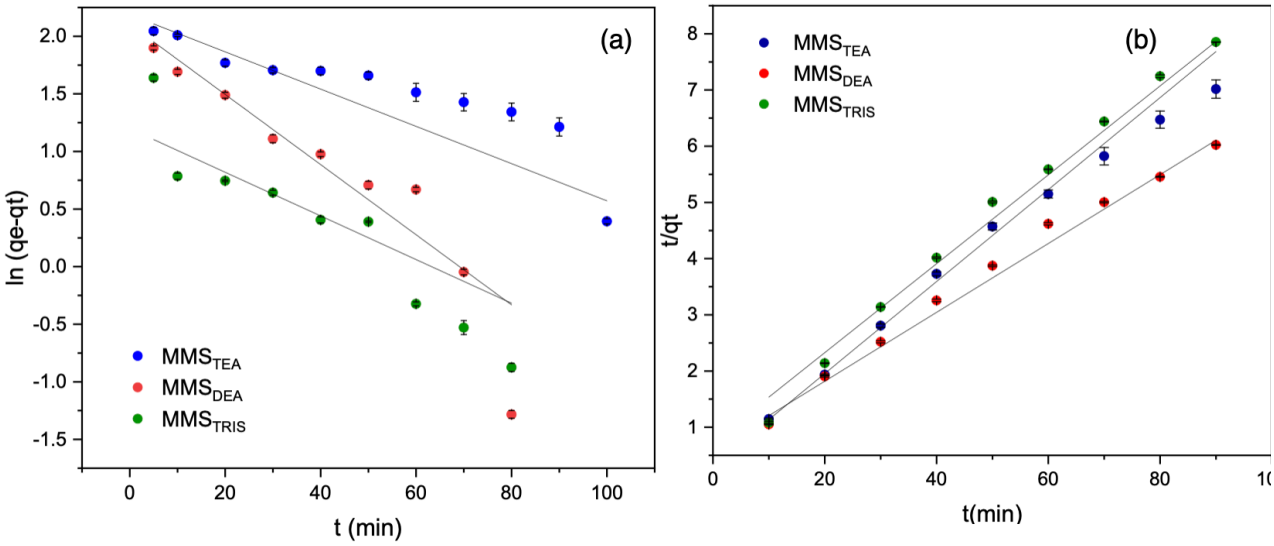

Fig. 3-8. Pseudo-first order kinetic (a) and Pseudo-second order kinetic (b) models of BG onto MMS composites.

The pseudo-second order rate constant of BG adsorption on MMS_{TRIS} is the highest among other composites, followed by the rate constant of BG adsorption on MMS_{TEA} and MMS_{DEA}. It is notable that the larger the average pore size of the composite, the higher the adsorption rate constant of BG on MMS composite.

Adsorption isotherms

The Langmuir and Freundlich isotherms models were used to describe the adsorption process of BG onto MMS composites. The Langmuir isotherm model assumes that the adsorption process is monolayer while the Freundlich isotherm model applies to multilayer adsorption process. The non-linear equations of Langmuir and Freundlich model were given in Eq. 5 and Eq. 6, respectively.

$$q_e = q_m K_L \frac{C_e}{1 + K_L C_e} \quad (5)$$

$$q_e = K_F C_e^{\,1/n} \quad (6)$$

Where C_e (mg L^{-1}) is the concentration of dye at equilibrium, q_e (mg g^{-1}) is the adsorption capacity at equilibrium, q_m (mg g^{-1}) is the maximum adsorption capacity, K_L (L mg^{-1}) is the Langmuir constant, K_F and n are the Freundlich adsorption constants.

The adsorption experiment data of BG onto all MMS composites were fitted using both isotherm models. The fitting curves were shown in **Fig. 3-9**. and the adsorption isotherm parameters were given in **Table 3-4**.

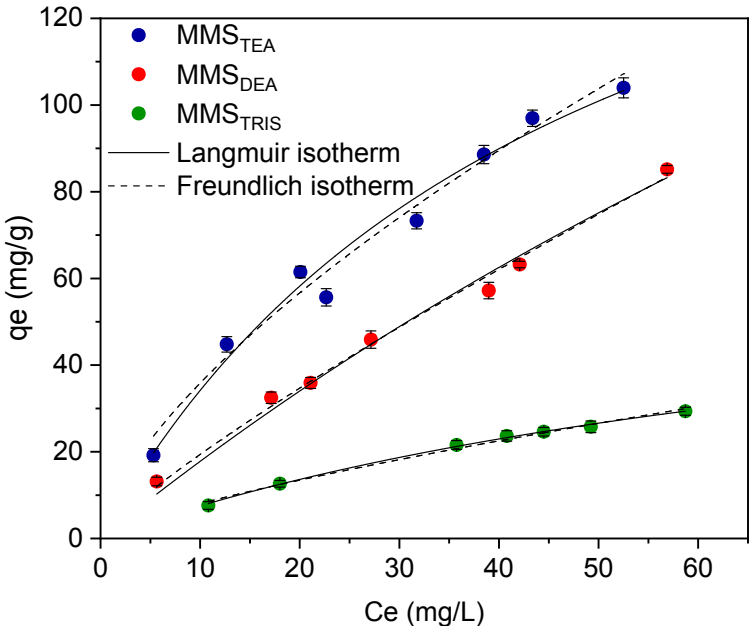

Fig. 3-9. Adsorption isotherms of BG onto MMS composites.

Table 3-4. Adsorption isotherm parameters of BG onto MMS composites.

Isotherm model	Parameters	Adsorbent		
		MMS_{TEA}	MMS_{DEA}	MMS_{TRIS}
Langmuir	q_m (mg g^{-1})	208.9	339.7	71.7
	K_L (L mg^{-1})	0.019	0.006	0.012
	R^2	0.979	0.988	0.998
Freundlich	K_F (mg $g^{-1}(mgL^{-1})^{-1/n}$)	21.36	3.69	1.72
	n	1.504	4.786	1.358
	R^2	0.980	0.993	0.992

The adsorption of BG onto MMS composites fitted well both Langmuir and Freundlich isotherm models (R^2>0.95) in the studied adsorptive concentration range. The 1/*n* value obtained from Freundlich isotherm was greater than 0 for all composites, indicating that the adsorption of BG on all prepared MMS composites were favorable.[23] The maximum adsorption capacity of BG onto all MMS composites in this work were comparable to some previously reported works (**Table 3-5**).

Table 3-5.Comparison of the maximum adsorption capacity of various adsorbents towards brilliant green dye.

Adsorbents	Adsorption capacity (mg g^{-1})	References
Areca nut husk	18.21	([24])
Ni-SBA-16	322.58	([25])
White rice husk	85.56	([26])
Chemically treated *Lawsoniainermis*seeds powder (CTLISP)	34.96	([27])
Polyurethane foam materials modified with coal (C/PUF)	134.95	([28])
MMS_{TEA}	208.9	This study
MMS_{DEA}	339.7	This study
MMS_{TRIS}	71.7	This study

Adsorption mechanism

Adsorption kinetic study suggested that the adsorption of BG onto MMS composites was mainly chemisorption process. Adsorption of BG onto MMS composites could involve electrostatic interaction between the protonated ammonium of BG molecule and the deprotonated hydroxyl group available on the surface of the composites. In addition, hydrogen bonding between hydroxyl groups of the adsorbent and amine group of BG can also proceed[29]

as illustrated in **Fig. 3-10**. Further study is necessary to elucidate a detailed adsorption mechanism of BG onto the prepared MMS composites.

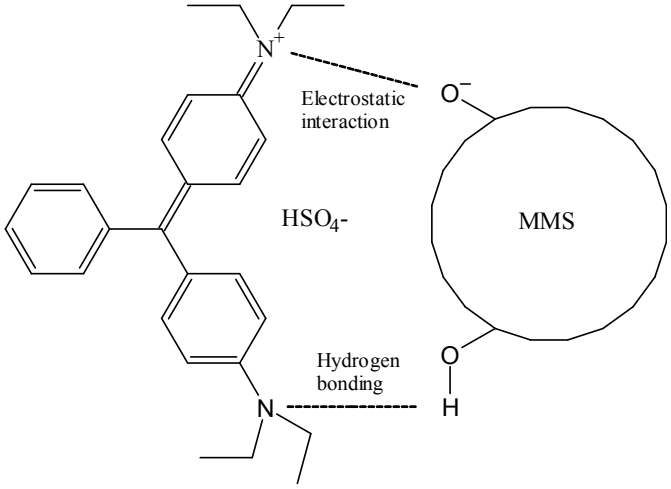

Fig. 3-10.Proposed adsorption mechanism of brilliant green onto MMS.

Recyclability

The regeneration ability of the MMS composites was studied since regeneration and recyclability properties of an adsorbent are crucial for the implementation in the real wastewater. The result of recyclability studies of all MMS composites was given in **Fig. 3-11**. The adsorption capacity of all MMS composites decreased quite significantly from one cycle to another. After the fourth cycle, the adsorption capacity of MMS decreased by 73%, 59%, 82% for MMS_{TEA}, MMS_{DEA}, and MMS_{TRIS}, respectively. However, after the third cycle, all composites still showed a good adsorption capacity of around 90-100 mg g^{-1}. A complete recovery of BG from MMS composite was hard to achieve, most likely due to the strong affinity of MMS for BG molecule. In addition, after sequential adsorption-desorption and washing processes, the active sites of MMS might be blocked or changed, causing the decrease of the adsorption capacity.

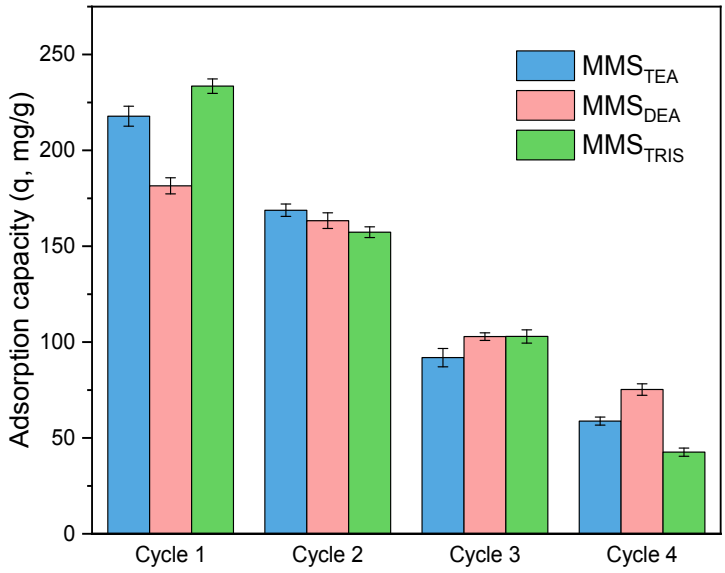

Fig. 3-11.Recyclability of MMS composites as adsorbents for BG.

3.4 Conclusions

Magnetic mesoporous silica (MMS) composites have been synthesized using various alkanaolamines as a basic catalyst in a one-pot system. The use of different alkanolamine resulted in MMS with different surface area, pore volume, and average pore size. The EDX, XRD, and XPS analysis showed the presence of magnetic nanoparticles in all composites. The application of the prepared composites for the removal of brilliant green (BG) from solution showed satisfactory results with excellent maximum adsorption capacities and adsorption rate. The main plausible mechanisms of adsorption of BG onto MMS were the chemical interaction such as hydrogen bonding and electrostatic interaction between BG and the hydroxyl groups of the composites. All of the prepared composites still showed high adsorption capacity towards BG after the third adsorption-desorption cycle. The results showed the potential of MMS as an adsorbent for the removal of BG dye from wastewater.

3.5 References

1. E. Zablocka-Godlewska and W. Prystaś, *Water Air Soil Pollut.*,**2020**,231, 1-23. https://doi.org/10.1007/s11270-020-4441-1.

2. O. Tunç, H. Tanaci, and Z. Aksu, *J. Hazard. Mater.*, **2009**,163**,** 187-198. https://doi.org/10.1016/j.jhazmat.2008.06.078.

3. S. H. Chen and A. S. Y. Ting, A.S.Y., *J. Environ. Manage.*,**2015**, 150, 274-280. https://doi.org/10.1016/j.jenvman.2014.09.014.

4. H. Li, S. Liu, J. Zhao, and N. Feng, *Colloids Surf. A: Physicochem. Eng. Aspects.*,**2016**, 494, 222-227. https://doi.org/10.1016/j.colsurfa.2016.01.048.

5. Y. Kang, H. Yoon, C. Lee, E. Kim, and Y. Chang, Y., *Water Res.*, **2019**, 151, 413-422. https://doi.org/10.1016/j.watres.2018.12.038

6. Y. Zhen, G. Yao, Q. Cheng, S. Yu, M. Liu, and C. Gao, *Desalination,* **2013**,328, 42-50. https://doi.org/10.1016/j.desal.2013.08.009.

7. B. K. Nandi, A. Goswami, and M. K. Purkait, *J. Hazard. Mater.*,**2009**,161,387-395. https://doi.org/10.1016/j.jhazmat.2008.03.110.

8. I. Konstantinou and T. A. Albanis, *Appl. Catal. B.*, **2004**, 49, 1-14. https://doi.org/10.1016/j.apcatb.2003.11.010.

9. M. T. Yagub, T. K. Sen, S. Afroze, and H. M. Ang, *Adv. Colloid Interface Sci.*, **2014**,209, 172-184. https://doi.org/10.1016/j.cis.2014.04.002.

10. V. K. Gupta, P. J. M. Carrott, M. M. L. RibeiroCarrott, and Suhas, *Crit. Rev. Env. Sci. Tec.*, **2009**, 39,783-842. https://doi.org/10.1080/10643380801977610.

11. V. B. Cashin, D. S. Eldridge, A. Yu, and D. Zhao, *Environ. Sci. Water Res. Technol.*, **2018**, 4, 110-128. https://doi.org/10.1039/C7EW00322F.

12. C. T. Kresge, M. E. Leonowicz, W. J. Roth, C. Vartuli, and J. S. Beck, *Nature*, **1992**, 359, 710-712. https://doi.org/10.1038/359710a0

13. J. Ye, D. Nyobe, B. Tang, L. Bin, P. Li, S. Huang, F. Fu, Y. Cai, G. Guan, and X. Hao, *J. Mol. Liq.*, **2020**, 303, 1-9. https://doi.org/10.1016/j.molliq.2020.112656

14. S. Egodawatte, A. Datt, E. A. Burns, and S. C. Larsen, *Langmuir*, **2015**, 31, 7553-7562. https://doi.org/10.1021/acs.langmuir.5b01483

15. R. K. Sharma, M. Yadav, and M. B. Gawande, *ACS Symp. Ser. Am. Chem. Soc*., **2016**, 1238, 1-38. https://doi.org/10.1021/bk-2016-1238.ch001

16. S. Nandy, D. Kundu, and M. K. Naskar, *J. Sol-Gel Sci. Technol*., **2014**, 72, 49-55. https://doi.org/10.1007/s10971-014-3420-7

17. M. Thommes, K. Kaneko, A. V. Neimark, J. P. Olivier F. Rodriguez-Reinoso, J. Rouquerol, and K. S. W. Sing, *Pure Appl. Chem.*, **2015**, 87, 1051-1069. https://doi.org/10.1515/pac-2014-1117

18. J. Kobler, K. Möller, and T. Bein, *ACS Nano*, **2008**, 2, 791-799. https://doi.org/10.1021/nn700008s

19. T. Radu, C. Iacovita, D. Benea, and R. Turcu, *Appl. Surf. Sci*., **2017**, 405, 337-343. https://doi.org/10.1016/j.apsusc.2017.02.002

20. M. Kokate, K. Garadkar, and A. Gole, *J. Mater. Chem. A*, **2013**, 1, 2022-2029. https://doi.org/10.1039/C2TA00951J

21. M. Ganguly and P. A. Ariya, *ACS Omega*, **2019**, 4, 12107-12120. https://doi.org/10.1021/acsomega.9b00757

22. A. Kamari, W. S. Wan Ngah, M. Y. Chong, and M. L. Cheah, *Desalination*, **2009**, 249, 1180-1189. https://doi.org/10.1016/j.desal.2009.04.010

23. M. A. Al-Ghouti and D. A. Da'ana, *J. Hazard. Mater*.,**2020**, 393, 1-22. https://doi.org/10.1016/j.jhazmat.2020.122383

24. K. S. Baidya and U. Kumar, *S. Afr. J. Chem. Eng*., **2021**,35, 33-43. https://doi.org/10.1016/j.sajce.2020.11.001

25. A. T. Shah, M. I. Din, F. N. Kanwal, and M. L. Mirza, *Arab. J. Chem*., **2015**,8, 579-586. https://doi.org/10.1016/j.arabjc.2014.11.046

26. M. P. Tavlieva, S. D. Genieva, V. G. Georgieva, and L. T. Vlaev, *J. Colloid Interface Sci.*, **2013**, 409, 112-122. https://doi.org/j.jcis.2013.07.052

27. R. Ahmad and K. Ansari, *Groundw. Sustain. Dev*., **2020**, 11, 1-9. https://doi.org/10.1016/j.gsd.2020.100417.

28. L. Kong, F. Qiu, Z. Zhao, X. Zhang, T. Zhang, J. Pan, and D. Yang, *J. Clean. Prod*., **2016**, 137, 51-59. https://doi.org/10.1016/j.jclepro.2016.07.067

29. R. Nicola, S.Muntean,M.Nistor,A.Putz., L.Almásy, and L.Săcărescu, *Chemosphere*, **2020**, 261, 1-14. https://doi.org/10.1016/j.chemosphere.2020.127737

Chapter 4

Microwave-assisted synthesis of magnetic silica-MIL-100(Fe) composite as an adsorbent for dye

Abstract

The composite of magnetic Fe_3O_4@SiO_2-MIL-100(Fe) was prepared by a microwave-assisted hydrothermal method and the adsorption properties of the composite for Congo red (CR) dye removal from aqueous solution was investigated. All components of the composite were synthesized under microwave irradiation. The synthesized materials were characterized by SEM, TEM, XRD, FTIR, BET, and TGA instruments. The characterization results indicated that the Fe_3O_4@SiO_2-MIL-100(Fe) composite was successfully synthesized. Adsorption studies demonstrated that the composite was highly selective for CR dye. The adsorption process of CR dye onto Fe_3O_4@SiO_2-MIL-100(Fe) followed the pseudo-second order kinetic model and better fitted the Freundlich isotherm model. The maximum adsorption capacity was found to be 277.2 mg g^{-1}, while for the bare MIL-100(Fe), the adsorption capacity towards CR dye was only 98.7 mg g^{-1}. The composite could be separated using an external magnet and could be recycled easily after the adsorption process, showing the potential for application in real industrial wastewater.

Keywords: microwave-assisted synthesis, magnetic particles, MIL-100(Fe), composite, adsorption of dye

4.1 Introduction

Dyes are among the top contaminants for water due to the extensive application in various fields. During the application, there is always a large part of the dyes that is discharged into the aqueous system.[1] Dyes are hazardous due to their high toxicity to humans and animals as well as their carcinogenic and mutagenic properties.[2,3] Therefore,

the removal of dyes from wastewater is considered important for environmental protection. Among the treatment technologies for dyes removal from aqueous system, adsorption is still highly preferable due to the economical reason, easy and simple technique, and high efficiency.[4] In the recent times, numerous adsorbents have been developed to remove the organic dyes from wastewater. One of which is the porous metal organic frameworks (MOFs). MOFs are highly porous frameworks which self-assemble to form coordination bonds between the transition metal cations and carboxylate anions. MOFs show high efficiency towards organic dyes removal due to the high specific surface area, size of accessible pores, the availability of adsorption sites, the electrostatic interaction, $\pi - \pi$ interaction and hydrogen bonding between the aromatic rings of MOFs and the aromatic ring of organic dyes.

Among various types of MOFs, the MIL-100(Fe) (Material of Institute Lavoiser) has some merits to be used in removal of dye from water such as its excellent water stability, high thermal stability, mesoporous structures enable easy and rapid diffusion of dye molecules, and the use of iron as a cation which is cheap, non-toxic and environmentally friendly.[5,6] In order to enhance the merits of the MOFs, the combination of MOFs with other functional material is considered a good approach. One of the potential materials for the integration with MOFs is magnetic Fe_3O_4@SiO_2 nanoparticles.

The combination of MIL-100(Fe) and magnetic Fe_3O_4@SiO_2 could facilitate the efficient separation and recycling of the used adsorbent by means of the magnetic properties. This will eliminate the tedious filtration or centrifugation process needed after the adsorption process. In addition, the synergistic effect between each material is expected to be able to enhance the adsorption efficiency towards organic dyes.

MOFs and their composites are mostly synthesized via hydrothermal strategy which requires hours even days for the synthesis.[7] Another strategy using microwave synthesis offers some advantages such as fast crystallization, high dispersion, shorter reaction time, and efficient control for particle and pore size distribution.[8] Synthesis of magnetic MOFs

composite under microwave irradiation will allow the synthesis for large scale application. Therefore, in this study, the preparation and characterization of Fe_3O_4@SiO_2-MIL-100(Fe) composite were done under microwave irradiation and the performance of the synthesized composite for organic dyes removal from water was evaluated.

4.2 Materials and methods

4.2.1 Materials

All chemicals used in the experiments were of analytical grade and were used as purchased. Iron(II)sulfate heptahydrate ($FeSO_4.7H_2O$) was obtained from Nacalai Tesque, INC (Kyoto, Japan). Iron(III)chloride hexahydrate ($FeCl_3.6H_2O$), 0.1 M NaOH, and ethanol were purchased from FUJIFILM Wako Pure Chemicals Corporation (Osaka, Japan). 28% ammonia, methylene blue (MB), and phenol red (PR) were purchased from Nacalai Tesque, INC (Kyoto, Japan). Tetraethyl orthosilicate (TEOS), amino propyl trimethoxysilane (APTMS), trimesic acid, and methyl violet (MV) were from Tokyo Chemical Industry Co., Ltd. (Tokyo, Japan). Congo red (CR) and brilliant green (BG) were obtained from FUJIFILM Wako Pure Chemicals Corporation (Osaka, Japan). Deionized water was used to prepare all the solutions.

4.2.2 Synthesis of Fe_3O_4 nanoparticles

Magnetic Fe_3O_4 nanoparticles were synthesized by mixing $FeSO_4$ and $FeCl_3$ in 40 mL H_2O. 20 mL of 0.1M NaOH solution was added to the mixture. The mixture was then put inside a microwave reactor (80ºC, 300 W) for 300 s. The produced black powder was washed with H_2O to neutral and dried at 60ºC overnight.

4.2.3 Synthesis of Fe_3O_4@SiO_2-NH_2nanoparticles

Fe_3O_4@SiO_2-NH_2 nanoparticles were also synthesized under microwave irradiation by dissolving 200 mg of the previously synthesized Fe_3O_4 nanoparticles in the mixture of 20

mL H_2O, 5 mL ethanol and 0.5 mL of dilute HNO_3. The solution was stirred and heated to 80ºC and 1 mL of TEOS was added drop wisely. The mixture was then put inside a microwave reactor and heated for 1800 s (80ºC, 300 W). As much as 0.3 mL of APTMS was drop wisely added to the mixture and the microwave irradiation was continued for another 180 s (60ºC, 300 W). The product was washed to neutral with H_2O and oven dried at 60ºC for overnight.

4.2.4 Synthesis of Fe_3O_4@SiO_2-MIL-100(Fe)

In order to synthesis the composite Fe_3O_4@SiO_2-MIL-100(Fe), 100 mg of the as synthesized Fe_3O_4@SiO_2-NH_2, $FeCl_3.6H_2O$, trimesic acid, and H_2O were mixed well and put inside the microwave reactor for 900 s (100º, 300W). The powder was washed with ethanol and H_2O at 70ºC for 6 h. The illustration of magnetic Fe_3O_4@SiO_2-MIL-100(Fe) composite synthesis was given in **Fig. 4-1**.

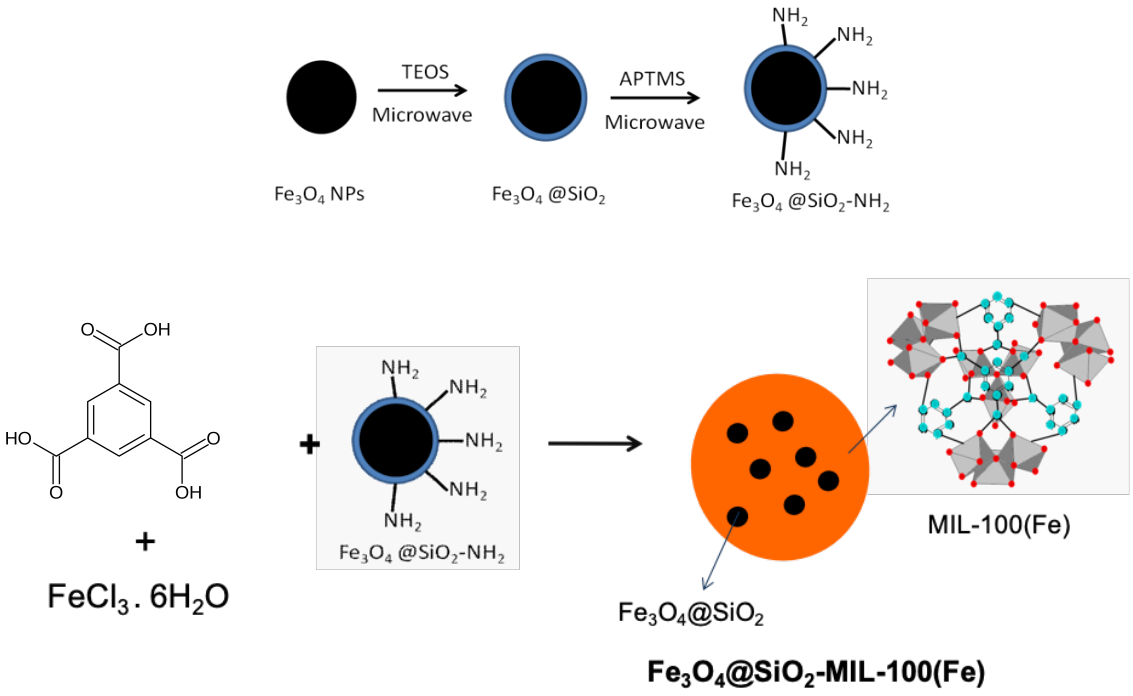

Fig. 4-1. Microwave-assisted synthesis of magnetic Fe_3O_4@SiO_2-MIL-100(Fe) composite.

4.2.5 Characterization

The surface morphology of the materials was analyzed using a scanning electron microscope (SEM, Hitachi, S-4300) instrument. The average size and morphology of the materials were investigated using a transmission electron microscope (TEM, JEOL, JEM-2100). The specific surface area, total pore volume, and pore size of the materials were determined by N_2 adsorption-desorption isotherm at 77K using a micrometer (Tristar II 3020, Micrometrics). The presence of functional groups in the materials was characterized using afourier-transform infrared spectroscopy (FTIR, Perkin Elmer Spectrum 400) instrument. The phase structure of the materials was characterized by using an X-ray powder diffraction (XRD, RigakuUltima II/PC) instrument with CuK_{α} radiation. Thermal stability was studied using thermogravimetric analyzer (TG/DTA 6300, S II Exstar).

4.2.6 Adsorption experiment

To choose the dye to be used as a model pollutant, the prepared magnetic Fe_3O_4@SiO_2-MIL-100(Fe) (2.5 mg) composite was mixed into aqueous solution of various dyes (20 mg L^{-1}, 10 mL) such as MB, CR, BG, PR, and MV. The chemical structure of each dye is given in **Table 4-1**. The composite was allowed to adsorb dyes without stirring at room temperature for 24 h in order to see the selectivity of the composite for each dye. The dye remained in each solution was analyzed using UV-visible spectrophotometer instrument.

Table 4-1. Chemical structure of various organic dyes in this study.

Dyes	Chemical structure
Brilliant green	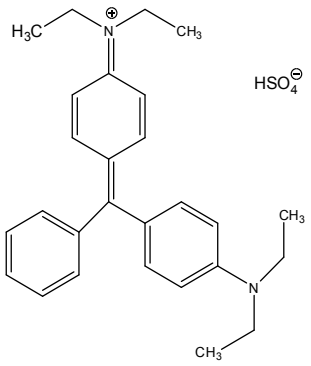
Congo red	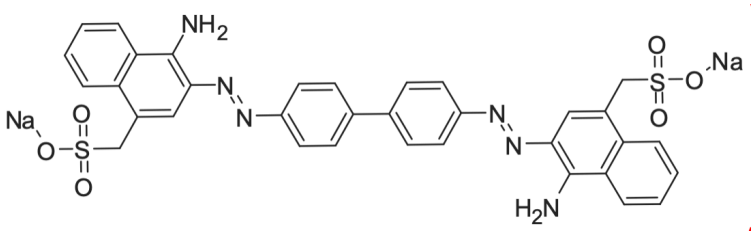
Methyl violet	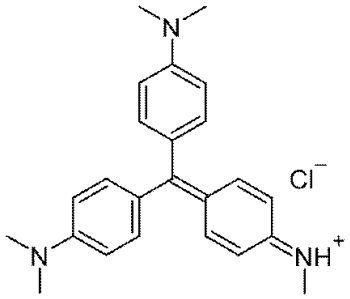
Methylene blue	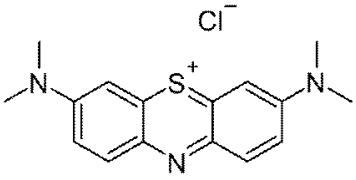
Phenol red	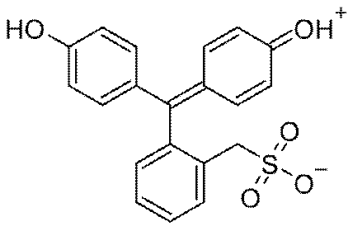

From the result of selectivity study, CR was further investigated as a model pollutant to study the adsorption properties of Fe_3O_4@SiO_2-MIL-100(Fe) composite towards organic dye. The adsorption process was performed in a batch system, in a constant solution volume of 10 mL and adsorbent amount of 4 mg. All adsorption experiments were conducted under the original pH of the solution and under room temperature, except stated otherwise. For the adsorption kinetic studies, the initial concentration was set to 20 mg L^{-1} and the interaction times were varied between 5-120 min. The adsorption isothermal studies were carried out under different initial concentrations of CR dye. The CR concentrations before and after adsorption process were measured using UV-visible spectrophotometer at a wavelength of 497 nm. The amount of dye adsorbed onto the composite was calculated using equation (1).

$$q_e = \frac{V(C_0 - C_e)}{m} \quad (1)$$

Where q_e (mg g^{-1}) is the adsorbed amount at equilibrium, C_o (mg L^{-1}) is the initial concentration of CR, C_e (mg L^{-1}) is the concentration of CR in aqueous solution at equilibrium; V is the volume of solution (L), and m is the adsorbent mass (g). Adsorption kinetics was studied using several kinetic models such as pseudo-first order kinetic model, pseudo-second order kinetic model, and intra-particle diffusion model.

The equation for pseudo-first order model is defined as equation (2)

$$\ln(q_e - q_t) = \ln q_e - k_1 t \quad (2)$$

The equation for pseudo-second order model is defined as equation (3):

$$\frac{t}{q_t} = \frac{1}{k_2 q_e^2} + \frac{t}{q_e} \quad (3)$$

The equation for intra-particle diffusion is defined as equation (4):

$$q_t = k_i t^{1/2} + C \quad (4)$$

In these equations, q_e (mg g^{-1}) and q_t (mg g^{-1}) are the adsorbed amount at equilibrium and time t, respectively, and k_1 (min^{-1}), k_2 (g mg^{-1} min^{-1}), k_i (mg g^{-1} $min^{-1/2}$) are the adsorption rate constants for pseudo-first order, pseudo-second order, and intra-particle diffusion models, respectively. *C* is the intercept of the linear graph.

Adsorption isothermal studies were fitted using Langmuir isothermal model and Freundlich isothermal model. The non-linear equations of Langmuir and Freundlich model were given in equation (5) and equation (6), respectively.

$$q_e = q_m K_L \frac{C_e}{1 + K_L C_e} \tag{5}$$

$$q_e = K_F C_e^{1/n} \tag{6}$$

Where C_e (mg L^{-1}) is the concentration of dye at equilibrium, q_e (mg g^{-1}) is the adsorbed amount of dye at equilibrium, q_m (mg g^{-1}) is the maximum adsorption capacity, K_L (L mg^{-1}) is the Langmuir constant, K_F is the Freundlich adsorption constants, and n is the dimensionless exponent of Freundlich equation.

The recyclability of Fe_3O_4@SiO_2-MIL-100(Fe) composite as an adsorbent for CR dye was also investigated by employing dilute NaOH solution to desorb CR from the composite. After sequential washing using distilled water and oven-drying, the adsorbent was reused for adsorption of CR in solution. This adsorption-desorption process was carried out for 3 cycles.

4.3 Results and discussion

4.3.1 Characteristics of Fe_3O_4@SiO_2-MIL-100(Fe)

The SEM images of Fe_3O_4@SiO_2, MIL-100(Fe), and Fe_3O_4@SiO_2-MIL-100(Fe) were illustrated in **Fig. 4-2**a-c. Fe_3O4@SiO_2 nanoparticles showed uniform spherical particles with the size in the range of 30-40 nm. The TEM images of MIL-100(Fe) and Fe_3O_4@SiO_2-MIL-100(Fe) in **Fig. 4-2**d,e showed the porous structures of both materials. It was seen

that Fe_3O_4@SiO_2 nanoparticles were successfully incorporated to MIL-100(Fe). The average sizes of Fe_3O_4@SiO_2 nanoparticles inside the composite were similar to the average size obtained from SEM images of Fe_3O_4@SiO_2.

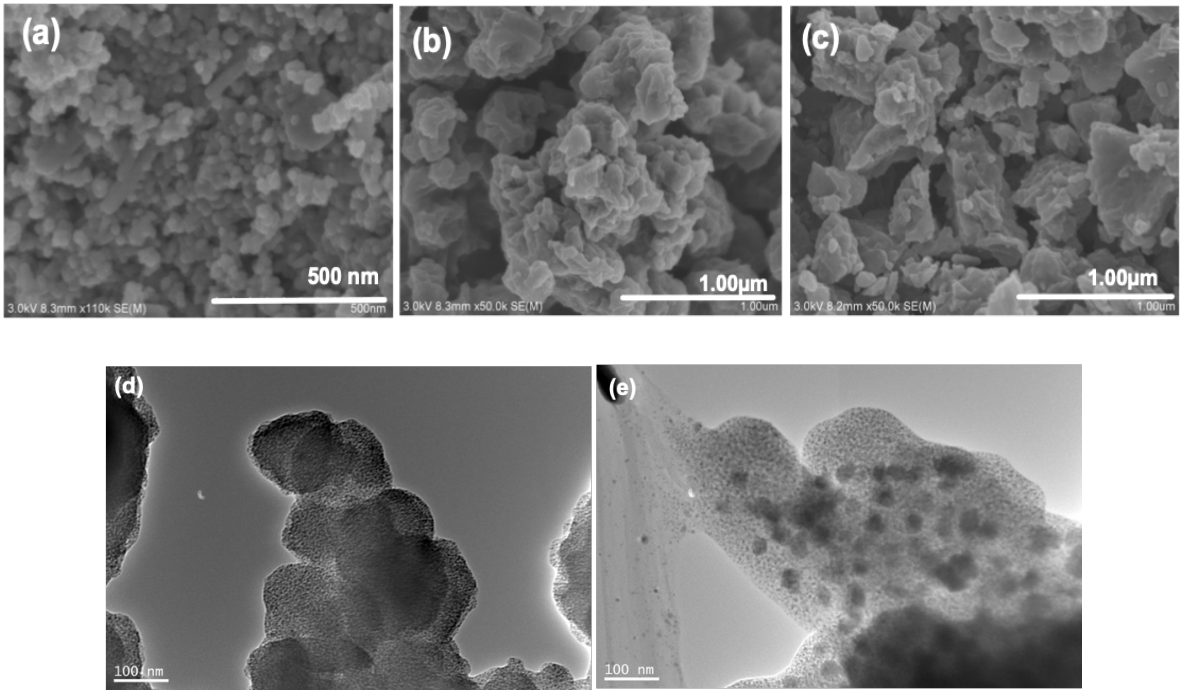

Fig. 4-2.SEM images of Fe_3O4@SiO_2 nanoparticles (a); MIL-100(Fe) (b); Fe_3O_4@SiO_2-MIL-100(Fe) (c); TEM images of MIL-100(Fe) (d); Fe_3O_4@SiO_2-MIL-100(Fe) (e).

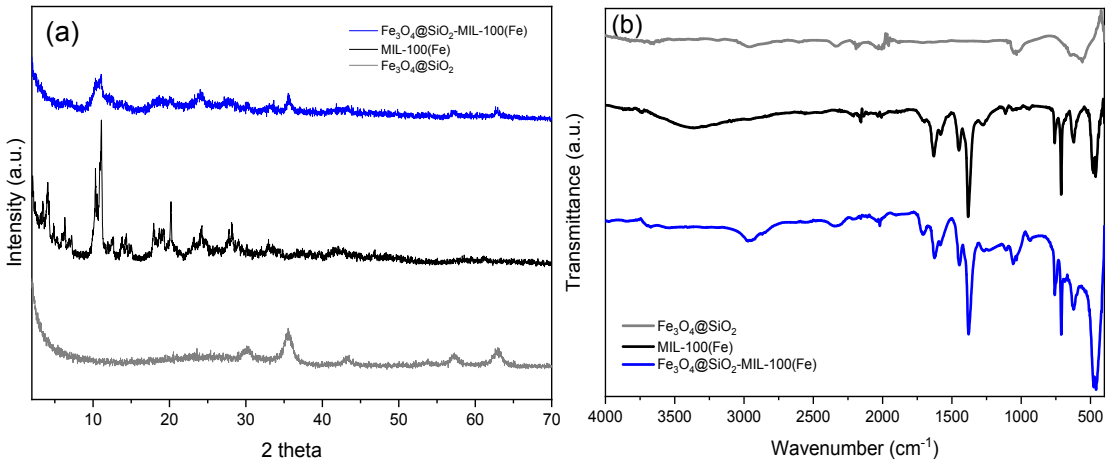

Fig. 4-3. XRD diffractogram (a); FTIR spectra (b); N_2 adsorption-desorption isotherm (c); and TGA curve (d) of the adsorbents.

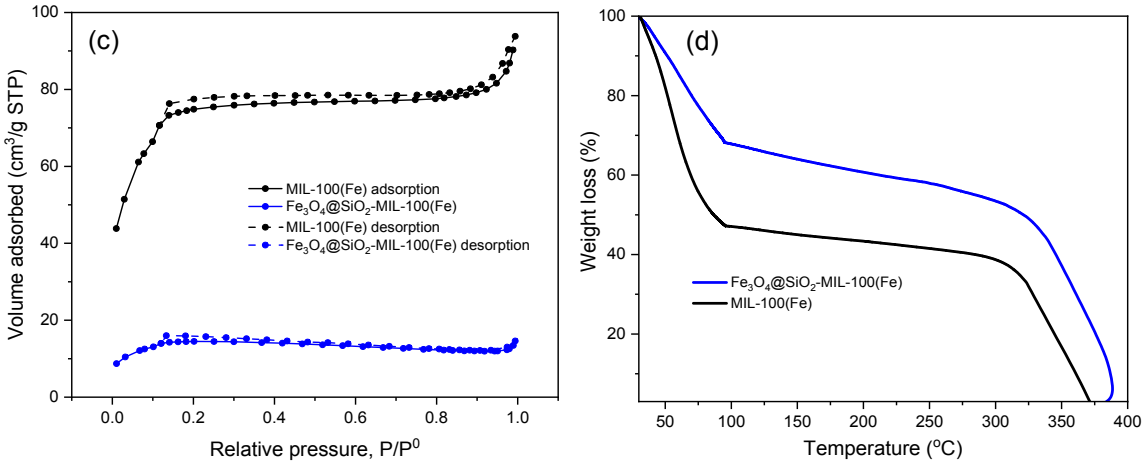

Fig. 4-3. (continuation) XRD diffractogram (a); FTIR spectra (b); N_2 adsorption-desorption isotherm (c); and TGA curve (d) of the adsorbents.

The XRD patterns of Fe_3O_4@SiO_2 nanoparticles, bare MIL-100(Fe), and Fe_3O_4@SiO_2-MIL-100(Fe) composite were shown in **Fig. 4-3**a. The diffraction peaks of Fe_3O_4@SiO_2-MIL-100(Fe) composite showed the combination of diffraction peaks of Fe_3O_4@SiO_2 and bare MIL-100(Fe). The diffraction peaks at 2θ = 30.1º, 35.4º, 43.4º, 53.5º, 57.2º, and 62.6º which corresponds (220), (311), (400), (422), (511), and (440) planes, respectively, confirmed the presence of magnetic Fe_3O_4 in the composites (JCPDS:75-0033). The diffraction peaks of the as synthesized MIL-100(Fe) were in a good agreement with some reported studies.[9,10] Diffraction peaks of both Fe_3O_4@SiO_2 and pristine MIL-100(Fe) were present in the XRD patterns of Fe_3O_4@SiO_2-MIL-100(Fe) composite, indicating the successful formation of the composite.

The FTIR spectra of Fe_3O_4@SiO_2 nanoparticles, bare MIL-100(Fe), and Fe_3O_4@SiO_2-MIL-100(Fe) composite were presented in **Fig. 4-3**b. The FTIR spectra of Fe_3O_4@SiO_2-MIL-100(Fe) showed absorption peak at 1033 cm^{-1} which corresponds to the absorption of Si-O-Si stretching vibration. This absorption peak was not present in the spectra of bare MIL-100(Fe). The absorption band at 1382 cm^{-1} corresponds to the symmetric –COOH

stretching and the strong vibration at 1636 cm^{-1} is attributed to the interaction between the deprotonated –COOH and the iron cation.[11]

Table 4-2. Physical properties of MIL-100(Fe) and Fe_3O_4@SiO_2-MIL-100(Fe).

Materials	BET surface area(m^2/g)	Pore volume (cm^3/g)	Average pore size (nm)
MIL-100(Fe)	269.4	0.14	2.1
Fe_3O_4@SiO_2-MIL-100(Fe)	51.7	0.02	1.6

Fig. 4-3c showed the N_2 adsorption-desorption isotherms of Fe_3O_4@SiO_2-MIL-100(Fe) and pristine MIL-100(Fe) synthesized under microwave irradiation. The BET specific surface area, the pore volumes and the average pore sizes were listed in **Table 4-2**. A sharp increase in the amount of N_2 adsorption at low pressure (P/P^o=0 - 0.1) indicated the presence of micropores in the materials. Both adsorption-desorption isotherm curves of MIL-100(Fe) and Fe_3O_4@SiO_2-MIL-100(Fe) exhibited type IV isotherms according to IUPAC classification, which was related to mesoporous materials.[12] In addition, the graph showed H4-type hysteresis loops which were generally found in complex materials containing both micropores and mesopores.[13] The specific surface area and pore volumes of Fe_3O_4@SiO_2-MIL-100(Fe) were significantly lower than those of the pristine MIL-100(Fe), which was due to the heavier cores of Fe_3O_4@SiO_2 in Fe_3O_4@SiO_2-MIL-100(Fe) composite.[14]

Thermal stability of the composite Fe_3O_4@SiO_2-MIL-100(Fe) and bare MIL-100(Fe) was studied at temperature range of 30ºC – 400ºC. The analysis result presented in **Fig. 4-3**d showed 2 steep decreases of weight during the heating process; from temperature 30ºC to 100ºC and at temperature higher than 325ºC. The weight loss at temperature 30ºC to 100ºC was due to the evaporation of water molecule that physically trapped inside the framework. At this temperature range, the weight loss of bare MIL-100(Fe) was higher than that of the composite Fe_3O_4@SiO_2-MIL-100(Fe), indicating the higher amount of water

molecule inside the pores of bare MIL-100(Fe). At temperature 100ºC-325ºC, the small weight loss was due to the release of H_2O molecule attached to iron trimers. At temperature higher than 325ºC, pyrolisis of the ligand H_3BTC started to occur, leading to the structural collapse of the material. From the TG analysis, it can be seen that the composite Fe_3O_4@SiO_2-MIL-100(Fe) was stable up to temperature 325ºC.

4.3.2 Adsorption studies

Selectivity for dyes

MB, CR, BG, PR, and MV were chosen to decide the dye model pollutant for Fe_3O_4@SiO_2-MIL-100(Fe) composite. It was seen that CR solutions become almost colorless (**Fig. 4-4**a) within 24 h even without the stirring process. Other dyes showed less adsorption onto Fe_3O_4@SiO_2-MIL-100(Fe) composite. The visible absorption spectrum of each dye before and after the addition of composite was given in **Fig. 4-4**b. It was obvious that Fe_3O_4@SiO_2-MIL-100(Fe) composite was selective towards the adsorption of CR. Thus, CR was chosen as a model pollutant to further study the adsorption properties of Fe_3O_4@SiO_2-MIL-100(Fe) composite. The inset in **Fig. 4-4**b showed that the Fe_3O_4@SiO_2-MIL-100(Fe) composite could be easily separated using an external magnetic bar.

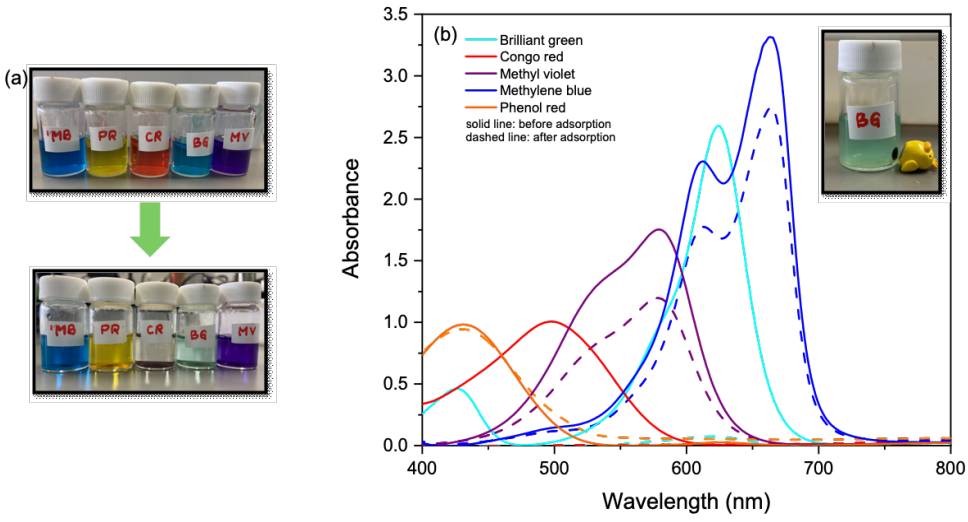

Fig. 4-4. Various dye solution before and after addition of Fe_3O_4@SiO_2-MIL-100(Fe) (a); UV-visible spectra of dyes before and after adsorption process (b).

Adsorption kinetics

Fig. 4-5a and **4-5**b showed the plotting curves for pseudo-first order kinetic and pseudo-second order kinetic models of CR adsorption onto the studied adsorbents. All the kinetic parameters are listed in **Table 4-3**. It can be seen that the adsorption of CR onto both MIL-100(Fe) and Fe_3O_4@SiO_2-MIL-100(Fe) are better fitted the pseudo-second order kinetic model. It could be assumed that the adsorption of CR onto both adsorbents involved chemical process or chemisorptions.[15]

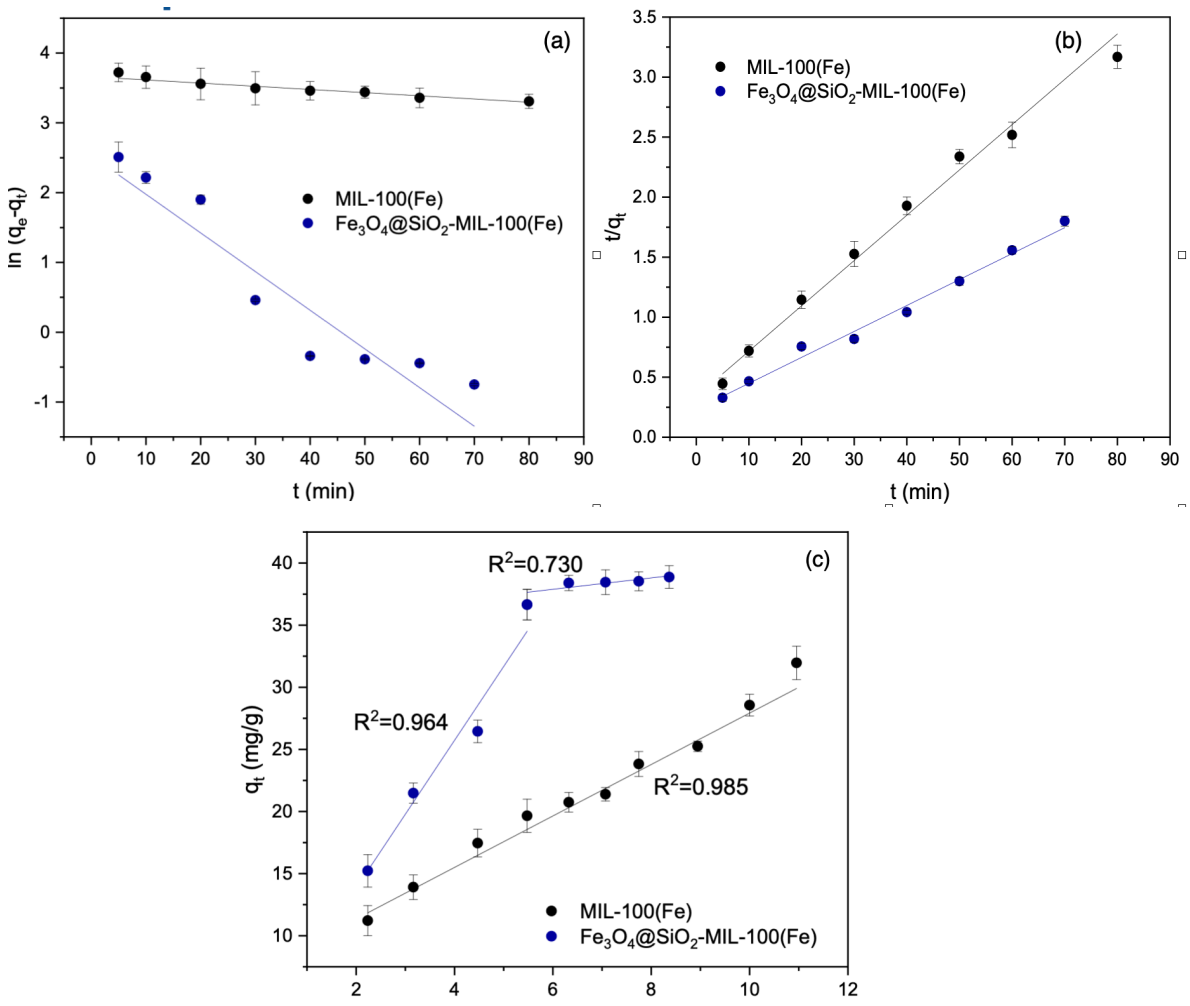

Fig. 4-5. Pseudo-first order (a); pseudo-second order (b); and intra-particle diffusion (c) kinetic models.

It is worth noticing that the adsorption rate of CR onto bare MIL-100(Fe) was slightly higher than that of the Fe_3O_4@SiO_2-MIL-100(Fe) composite. The possible reason is because the larger pore size of the pristine MIL-100(Fe) will cause a faster diffusion of the dye molecule into the adsorbent.[16]

Intra-particle diffusion model was used to study the diffusion mechanism and the rate-limiting step of the adsorption process of dye.[17] For CR dye adsorption onto pristine MIL-100(Fe), **Fig. 4-5**c showed a linear graph, indicating that the adsorption process of CR onto MIL-100(Fe) occurred in a one-stage adsorption process. However, the linear graph does not pass the origin, suggesting that the adsorption process is influenced by intra-particle diffusion together with other kinetic effects.[18] For CR adsorption onto Fe_3O_4@SiO_2-MIL-100(Fe) composite, the graph showed two linear lines which suggested that the adsorption process of CR onto the composite could be divided into two stages.[19] The first stage is the transport of the dye mass to the outer space of the composite and the second stage is the slow diffusion of CR dye molecules inside the pore channels of the composite.[20]

Table 4-3. Kinetic parameters of CR adsorption onto the prepared adsorbents.

Kinetic models	Parameters	Adsorbents	
		MIL-100(Fe)	Fe_3O_4@SiO_2-MIL-100(Fe)
Pseudo-first order	k_1 (min^{-1})	5.31×10^{-3}	5.41×10^{-2}
	R^2	0.942	0.891
Pseudo-second order	k_2 (g mg^{-1} min^{-1})	3.37×10^{-3}	2.09×10^{-3}
	q_e (mg g^{-1})	27.6	45.7
	R^2	0.990	0.990
Intra-particle diffusion	k_{i1}(mg g^{-1} $min^{-1/2}$)	2.19	3.43
	k_{i2}(mg $g^{-1}min^{-1/2}$)	-	1.63
	C_1	6.84	1.06
	C_2	-	33.60
	R_1^2	0.986	0.964
	R_2^2	-	0.730

Adsorption isotherm

Adsorption isotherms describe the equilibrium relation between the adsorbed dye (q_e) and the dye concentration (C_e) at constant temperature and pH. The adsorption isotherms were determined by fitting the experimental data with non-linear Langmuir and Freundlich isotherms. The fitting curves are given in **Fig. 4-6**a and **4-6**b and all the isotherm parameters are given in **Table 4-4**. The correlation coefficient values of CR onto bare MIL-100(Fe) and Fe_3O_4@SiO_2-MIL-100(Fe) composite were better fitted the Freundlich isotherm models with the R^2 values of 0.976 and 0.971 for MIL-100(Fe) and Fe_3O_4@SiO_2-MIL-100(Fe), respectively. Freundlich isotherm is used to describe non-ideal, multilayer and reversible adsorption at a heterogenous surface. The 1/*n* values of both adsorbents are less than 1, indicating the chemisorption process.[15] The Langmuir maximum adsorption capacity (q_{max}) of Fe_3O_4@SiO_2-MIL-100(Fe) composite for CR dye is 277.2 mg g^{-1}, which is much higher than that of the MIL-100(Fe). The adsorption capacity of Fe_3O_4@SiO_2-MIL-100(Fe) composite for CR dye is comparable with that of other reported magnetic adsorbents as listed in **Table 4-5**.

Although the Fe_3O_4@SiO_2-MIL-100(Fe) composite has much lower BET surface area and pore volume, it shows much better adsorption performance than MIL-100(Fe). This result indicated that the adsorption capacity was not solely determined by the porosity and surface area of the adsorbents. In addition, the adsorption process of CR onto the MIL-100(Fe) and Fe_3O_4@SiO_2-MIL-100(Fe) is mainly due to the electrostatic interaction between the CR dye and the adsorbents.[21]

Table 4-4. Isotherm parameters of CR adsorption onto the adsorbents.

Adsorbent	Langmuir isotherm			Freundlich isotherm		
	q_m (mg g^{-1})	K_L (L mg^{-1})	R^2	K_F (mgL^{-1})	*n*	R^2
MIL-100(Fe)	98.7	0.525	0.836	3.778	4.679	0.976
Fe_3O_4@SiO_2-	277.2	0.809	0.966	18.060	2.62	0.971

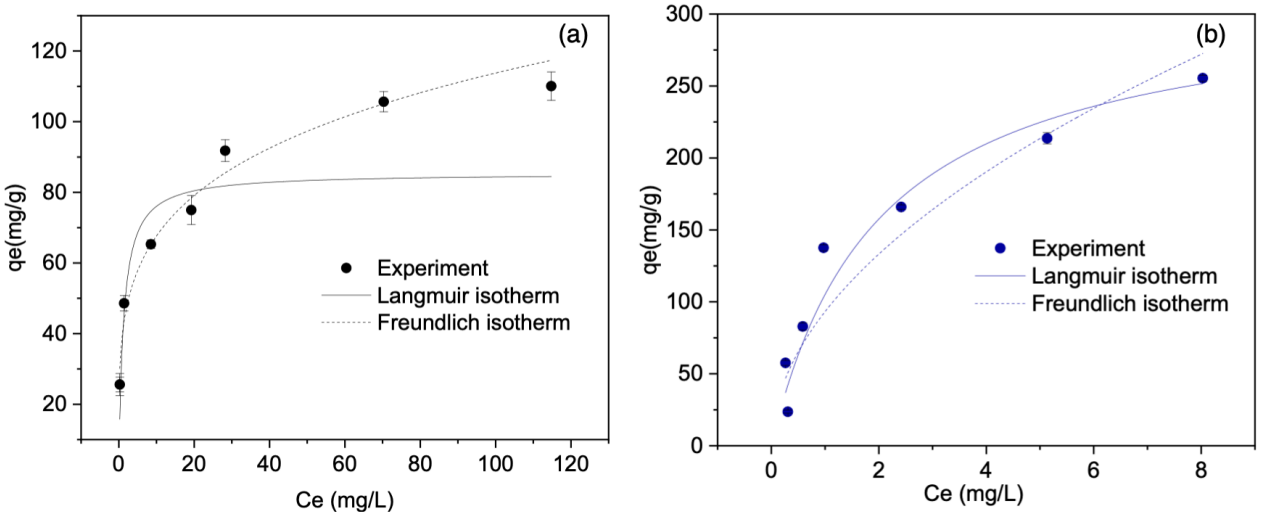

Fig. 4-6. Adsorption isotherm parameter plots for MIL-100(Fe) (a) and Fe_3O_4@SiO_2-MIL-100(Fe) (b).

Table 4-5. Comparison maximum adsorption capacity of various magnetic adsorbents for Congo red dye.

No.	Adsorbents	Adsorption capacity, q_m (mg g^{-1})	References
1.	Magnetic core-manganese oxide shell nanoparticles	42.00	(22)
2.	Magnetic chitosan composite microparticles (MCCPs)	263.16	(23)
3.	Magnetic mesoporous titanium dioxide-graphene oxide	89.95	(24)
4.	Magnetic cellulose/Fe_3O_4/activated carbon composite	66.09	(25)
5.	Magnetic Fe_3O_4@graphene composite (FGC)	33.66	(26)
6.	Magnetic alginate/γ-Fe_2O_3/Cds nanocomposite	20.31	(27)
7.	Fe_3O_4@SiO_2-MIL-100(Fe)	277.2	This study

Plausible adsorption mechanism

From these experiments, it was suggested that the adsorption process of CR onto Fe_3O_4@SiO_2-MIL-100(Fe) composite was mainly due to the electrostatic interaction between dye and composite adsorbent molecules. Besides, the presence of aromatic rings on the composite and CR dye molecule will provide $\pi - \pi$ stacking interaction between the composite and dye. The plausible adsorption mechanism of CR dye onto Fe_3O_4@SiO_2-MIL-100(Fe) composite was depicted in **Fig. 4-7**.

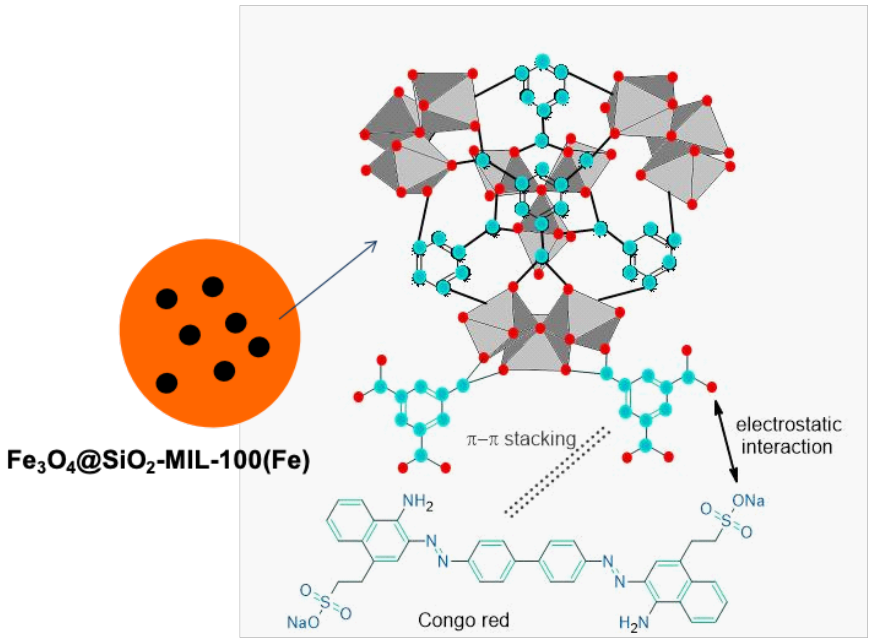

Fig. 4-7.Mechanism of CR adsorption onto Fe_3O_4@SiO_2-MIL-100(Fe) composite.

Recyclability

The recycling performance of an adsorbent is an important characteristic for the adsorbent to be used in the actual application. The adsorbed CR could be desorbed from Fe_3O_4@SiO_2-MIL-100(Fe) composite using dilute NaOH solution. CR dye is an acidic diazodye, therefore it is attracted towards alkaline medium. The removal efficiency of composite decreased gradually from around 30% to 70% from the second to the third cycle as shown in **Fig. 4-8**. This indicated that the CR dye are strongly bonded to the surface of composite and could not be desorbed totally with dilute NaOH. In addition, after

washing with water, a large fraction of pores on the composite became inaccessible to CR dye molecules. The Fe_3O_4@SiO_2-MIL-100(Fe) composite could be used for up to 2 cycles for adsorption of CR dye using dilute NaOH as a desorbing agent.

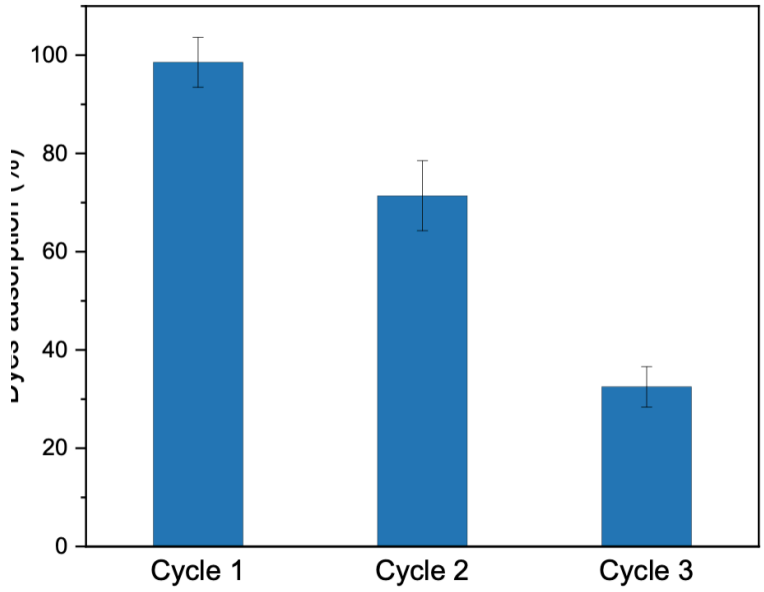

Fig. 4-8. Bar graph of the recyclability of Fe_3O_4@SiO_2-MIL-100(Fe).

4.4 Conclusion

The Fe_3O_4@SiO_2-MIL-100(Fe) composite has been synthesized under microwave irradiation. The characterization results showed that the Fe_3O_4@SiO_2 nanoparticles were incorporated to MIL-100(Fe) structure. The composite was selective for CR dye and showed better adsorption performance than the pristine MIL-100(Fe). The adsorption process of CR onto the Fe_3O_4@SiO_2-MIL-100(Fe) composite better fitted the pseudo-second order kinetic model and Freundlich isotherm model. A plausible adsorption mechanism of CR onto the Fe_3O_4@SiO_2-MIL-100(Fe) composite was also proposed in this study. The synthesized composite demonstrated advantages in terms of low cost, easy separation, high selectivity and efficiency for CR removal from water.

4.5 References

1. I. E. Uflyand, V. A. Zhinzhilo, V. O. Nikolaevskaya, B. I. Kharisov, C. M. O. González, and O. V. Kharissova, *Microchem. J*., 2021, 168, 106387. https://doi.org/10.1016/j.microc.2021.106787
2. F. R. Abe, J. N.Mendonça, L. A.Moraes, G. A. R. Oliveira, C. Gravato, A. M. V. Soares, and D. P. Oliveira, *Chemosphere*, 2017, 178, 282-290. https://doi.org/j.chemosphere.2017.03.030
3. X. Ren, G. Zeng, L. Tang, J. Wang, J. Wan, Y. Liu, H. Yi, S. Ye, and R. Deng, *Sci. Total Environ*., 2018, 610-611, 1154-1163. https://doi.org/10.1016/j.scitotenv.2017.08.089
4. M. Ismail, K. Akhtar, M. I. Khan, T. Kamal, M. A. Khan, A. M. Asiri, J. Seo, and S. B. Khan, *Curr. Pharm. Des*., 2019, 25, 3645-3663. https://doi.org/10.2174/1382566619102114202 6
5. Q. Gao, J. Xu, and X.Bu,*Coord. Chem. Rev*., 2019, 378, 17-31. https://doi.org/10.1016/j.ccr.2018.03.015
6. A. C. Tella, J. T. Bamgbose, V. O.Adimula, M.Omotoso, S. E. Elaigwu, V. T. Olayemi, and O. A. Odunola, *SN Appl. Sci*., 2021, 3, 136. https://doi.org/10.1007/s42452-021-04163-w
7. R. Seetharaj, P. V. Vandana, P. Arya, and S. Mathew, *Arab. J. Chem*., 2015, 12, 295-315. https://doi.org/10.1016/j.arabjc.2016.01.003
8. X. Wang, X. Zhao, D. Zhang, G. Li, and H. Li, *Appl. Catal. B Environ*.,2018, 228, 47-53. https://doi.org/10.1016/j.apcatb.2018.01.066
9. F. Ke, L.Qiu, and J.Zhu,*Nanoscale*, 2014, 6, 1596-1601. https://doi.org/10.1039/C3NR05051C
10. M. Chen, S. Zhou, Z.Xu, L. Ding, and Y. Cheng, *Molecules*, 2019, 24, 3718. https://doi.org/10.3390/molecules24203718

11. J. W. Yoon, Y. K.Seo, Y. K. Hwang, J. S. Chang, H. Leclerc, S.Wuttke, P.Bazin, A. Vimont, M.Daturi, E. Bloch, P. L. Llewellyn, C.Serre, P. Horcajada,J. M.Grenèche, A. E. Rodrigues, andG.Férey, *Angew. Chem. Int. Ed.*, 2010, 49, 5949-5952. https://doi.org/10.1002/anie.201001230

12. M. Thommes, K. Kaneko, A. V.Neimark, J. P.Olivier,F. Rodriguez-Reinoso, J. Rouquerol, and K. S. W. Sing, *Pure Appl. Chem*., 2015, 87, 1051-1069. https://doi.org/10.1515/pac-2014-1117

13. M. Thommes,*Chem. Ing. Tech*., 2010, 82, 1059-1073. https://doi.org/10.1002/cite.201000064

14. S. Yu, J. Wan, and K. Chen, *J.ColloidInterfaceSci*., 2016, 461, 173-178. https://doi.org/10.1016/j.jcis.2015.09.015

15. T. R. SahooandB.Prelot, Chapter 7 – Adsorption processes for the removal of contaminants from wastewater: the perspective role of nanomaterials and nanotechnology. In B. Bonelli, F. S., Freyria, I. Rossettii, R. Sethi (Ed.). *Micro and nano technologies, Nanomaterials for the detection and removal of wastewater pollutants* (pp. 161-222). Elsevier.2020.https://doi.org/10.1016/B978-0-12-818489-9.00007-4

16. D. Chen, Y. Cao, N. Chen, and P. Feng, *J. Inorg. Organomet. Polym. Mater.*,2020, 31, 1231-1240. https://doi.org/10.1007/s10904-020-01831-y

17. T. S. Lin, Z. L. Song, G. B.Che, A.Ren, P. Li, C. B. Liu, and J. S. Zhang, *MicroporousMesoporous Mater*., 2014, 193, 27-34. https://doi.org/10.1016/j.micromeso.2014.03.004

18. L. Tang, Y.Cai, G. Yang, Y. Liu, G.Zeng, Y. Zhou, S. Li, J. Wang, S. Zhang, Y. Fang, and Y. He, *App. Surf. Sci*., 2014, 314, 746-753. https://doi.org/10.1016/j.apsusc.2014.07.060

19. G. Feiqiang, L.Xiaolei, J.Xiaochen, Z.Xingmin, G. Chenglong, and R. Zhonghao, *Colloids Surf. A*, 2018, 555, 43-54. https://doi.org/10.1016/j.colsurfa.2018.06.061

20. X. Z. Guo, S. S. Han, J. M. Yang,X. M. Wang, S. S. Chen, and S. Quan, *Ind. Eng. Chem. Res*., 2020, 59, 2113-2122. https://doi.org/10.1021/acs.iecr.9b05715

21. C. Chen, M. Zhang, Q. Guan, and W. Li, *Chem. Eng. J*., 2012, 183, 60-67. https://doi.org/10.1016/j.cej.2011.12.021

22. Y. Zhai, J.Zhai, M. Zhou, and S. Dong, *J. Mater. Chem.,*2009, 19, 7030-7035. https://doi.org/10.1039/B912767D

23. P. Wang, T. Yan, and L. Wang, *BioResources*, 2013, 8, 6026-6043. https://doi.org/10.15376/biores.8.4.6026-6043

24. L. Li, X. Li, H.Duan, X. Wang, andC.Luo, *Dalton Trans*., 2014, 43, 8431. https://doi.org/10.1039/c3dt53474j

25. H. Y. Zhu, Y. Q. Fu, R. Jiang, J. H. Jiang, L. Xiao, G. M. Zeng, S. L. Zhao, and Y. Wang,*Chem. Eng. J*., **2011**, 173, 494-502. https://doi.org/10.1016/j.cej.2011.08.020

26. Y. Yao, S. Miao, S. Liu, L. P. Ma, H. Sun, and S. Wang, *Chem. Eng. J*., **2012**, 184, 326-332. https://doi.org/10.1016/j.cej.2011.12.017

27. R. Jiang, J. Yao, H. Zhu, Y. Fu, Y. Guan, L. Xiao, andG.Zeng, *Desalination Water Treat.*, **2014**, 52, 238-247. https://doi.org/10.1080/19443994.2013.787551

Chapter 5

Preparation and characterization of magnetic mesoporous silica@MIL-(Fe) composite for the removal of cationic and anionic dyes from water

Abstract

In this study, the composite of magnetic mesoporous silica (MMS) and MIL-100(Fe), MMS@MIL-100(Fe), has been synthesized using a hydrothermal method to remove anionic Congo red (CR) and cationic methylene blue (MB) dyes from aqueous solutions. The synthesized MMS@MIL-100(Fe) composite was thoroughly characterized by X-ray diffraction, Fourier transform infrared spectrophotometer, scanning electron microscopy, transmission electron microscopy and surface area analyzer. Results of the characterization suggested the presence of magnetic mesoporous silica in the framework of MIL-100(Fe). The studied adsorption parameters include interaction time and the initial concentration of dyes. The adsorption of CR and MB onto the MMS@MIL-100(Fe) composite was better explained with pseudo-second order kinetic model and Langmuir isotherm model. The adsorption studies showed a selectivity of MMS@MIL-100(Fe) composite towards MB dye with a maximum adsorption capacity (q_{max}) of 243.9 mg g^{-1} and a kinetic adsorption rate constant (k_2) of $1.9.10^{-2}$ $g.mg^{-1}.min^{-1}$. This suggested a potential of the composite for removing cationic dyes from real wastewater.

Keywords: *Metal-organic frameworks, Magnetic composite, Dye adsorption.*

5.1 Introduction

Synthetic dyes have been widely used in textile, cosmetics, leather, pharmaceutical, rubber, and plastic industries; thus, they are considered one of the top pollutants in water. Dyes could significantly affect the growth of animals and plants in water and could also affect human health due to their mutagenic and carcinogenic properties.[1] Therefore, the effective removal of

synthetic dyes from water is necessary. Various technologies have been applied to remove synthetic dyes from water such as chemical oxidation, photocatalytic degradation, adsorption, membrane filtration, and coagulation/flocculation. Among those technologies, adsorption is preferred due to its efficiency and simplicity.[2]

Numerous adsorbents have been used to remove synthetic dyes from water, such as activated carbon, bioadsorbents, nanomaterials, metal oxide-based materials, polymer composite and metal-organic frameworks (MOFs). MOFs have attracted attentions for pollutants removal in water due to their excellent properties including tuneable high specific surface area and pore volume.[3] Among the type of MOFs, MIL-100(Fe) is preferred for application in water due to its high water stability and thermal stability.[4] The corporation of MIL-100(Fe) with other functional materials is a good approach to increase the adsorption ability of the materials.

In this study, the composite consisted of magnetic mesoporous silica (MMS) and MIL-100(Fe), MMS@MIL-100(Fe), was developed to produce a powerful adsorbent for different synthetic dyes in water. Two types of dyes, cationic methylene blue (MB) and anionic Congo red (CR) were used as model pollutants for the adsorption process. The adsorption data were fitted with pseudo-first order and pseudo-second order kinetic models and Langmuir and Freundlich isotherm models to study the adsorption mechanism.

5.2 Materials and methods

5.2.1 Materials

All chemicals in this study were used as purchased. Iron(II)sulfate heptahydrate ($FeSO_4.7H_2O$), 28% ammonia, and methylene blue (MB) were purchased from NacalaiTesque, INC (Kyoto, Japan). Iron(III)chloride hexahydrate ($FeCl_3.6H_2O$), 1 M NaOH, cetyltrimethylammonium bromide (CTAB), ethanol, and Congo red (CR) were obtained from FUJIFILM Wako Pure Chemicals Corporation (Osaka, Japan). Tetraethyl orthosilicate (TEOS) and trimesic acid were from Tokyo Chemical Industry Co., Ltd. (Tokyo, Japan). Deionized water was used to prepare all the solutions.

5.2.2 Preparation of MMS

$FeSO_4.7H_2O$ (700 mg) was dissolved in 46 mL H_2O and $FeCl_3.6H_2O$ (1170 mg) was dissolved in 40 mL H2O. Both iron precursors solutions were mixed and added by 25 mL 1 M NaOH. The black mixture was stirred for 30 min and was referred as solution A. CTAB (0.672 mmol) was dissolved in 5 mL NaOH and was added to solution A. TEOS (4.48 mmol) was then added to the mixture drop wisely and stirred for 2h and left at room temperature for 24 h. After sub sequential washing with H_2O, the black product was dried at 60ºC for overnight. MMS powder was calcined at 500ºC for 5 h to remove the template.

5.2.3 Preparation of MMS@MIL-100(Fe)

MMS@MIL-100(Fe) was prepared by using a hydrothermal method. One hundred milligrams of the as-synthesized MMS was added into the MIL-100(Fe) precursor. The MIL-100(Fe) precursor was prepared by stirring 688 mg trimesic acid, 300 mg $FeCl_3.6H_2O$, 0.2 mL HF and 0.19 mL HNO_3 in 20 mL H_2O for 10 min. After immersing MMS powder into the solution, the mixture was transferred into a Teflon-lined autoclave and put into the oven at 150ºC for 12h. The produced light orange powder was sequentially washed with H_2O at 80ºC for 5h and EtOH at 60ºC for 3h. The schematic of the MMS@MIL-100(Fe) synthesis is given in **Fig. 5-1**. The pristine MIL-100(Fe) was synthesized with the same procedure except without the addition of MMS.

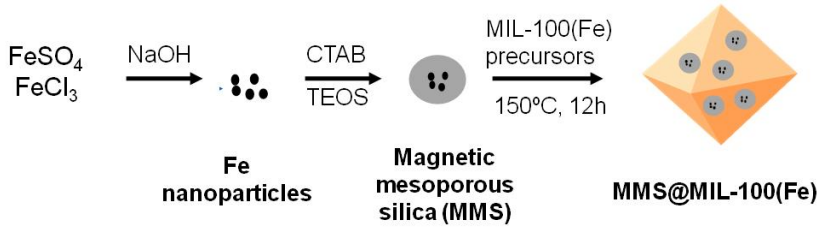

Fig. 5-1. Schematic diagram of the synthesis of MMS@MIL-100(Fe).

5.2.4 Characterizations

The morphology of the materials was investigated using a scanning electron microscope (SEM, Hitachi, S-4300) and a transmission electron microscope (TEM, JEOL, JEM-2100)

instruments. The specific surface area of the materials was determined by Brunauer-Emmett-Teller (BET) method based on the N_2 adsorption-desorption isotherm using a gas sorption analyzer (Tristar II 3020, Micrometrics). The presence of functional groups in the materials was characterized using a Fourier-transform infrared spectroscopy (FTIR, Perkin Elmer Spectrum 400) instrument. The phase structure of the composite was studied using an X-ray powder diffraction (XRD, Rigaku Ultima II/PC) instrument with CuKα radiation.

5.2.5 Adsorption experiments

In the adsorption studies, various concentrations of CR and MB solutions were prepared using deionized water. The adsorption process was carried out using batch systems under the original pH of the dye solutions. Adsorption kinetic data were obtained by immersing 10 mg of the adsorbent in 50 mL of 20 mg L^{-1} dye solution. At specified time intervals, the dye concentration remained in the solution was measured using a UV-vis spectroscopy (Hitachi, U-4100 Spectrophotometer). Adsorption isotherm was studied for 24 h using various initial concentrations of dyes and a specified volume of dye and mass of the adsorbent. The adsorption capacities of the adsorbents towards cationic MB and anionic CR were calculated using the equation (1):

$$q_e = \frac{(C_0 - C_e)}{m} V \quad (1)$$

Where C_0 and C_e (mg/L) are the initial and dye concentrations at a given time, respectively. Parameter V (L) is the volume of the solution and m (g) represents the mass of the adsorbent.

5.3 Results and discussion

5.3.1 Characterization of MMS@MIL-100(Fe)

The morphologies of MIL-100(Fe) and MMS@MIL-100(Fe) were observed by SEM and TEM as shown in **Fig. 5-2**. The SEM image of MIL-100(Fe) (**Fig.5-2**a) showed the octahedral shape of MOF and the MOFs' relatively uniform particle size. For the MMS@MIL-100(Fe)

composite in **Fig. 5-2**b, the octahedral shape is preserved with an occurrence of particles' agglomeration. The TEM images of MIL-100(Fe) in **Fig. 5-2**c showed that the particle size of MIL-100(Fe) was approximately 200 nm.The TEM image of MMS@MIL-100(Fe) composite in **Fig. 5-2**d showed the presence of MMS particle on the framework of MIL-100(Fe).

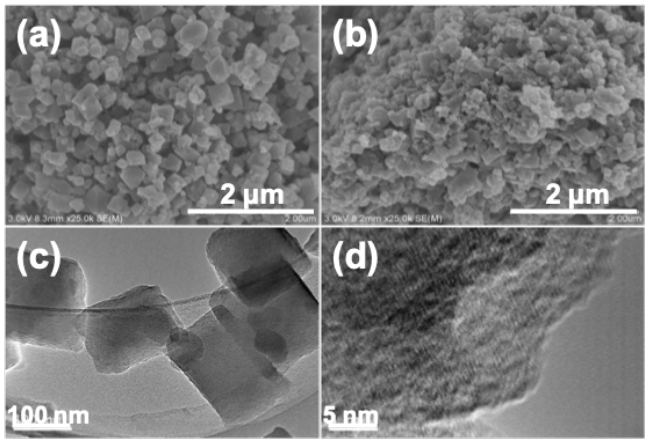

Fig. 5-2. SEM images of MIL-100(Fe) (a) and MMS@MIL-100(Fe) (b); TEM images of MIL-100(Fe) (c) and MMS@MIL-100(Fe) (d).

The XRD patterns of MMS, MIL-100(Fe) and MMS@MIL-100(Fe) are depicted in **Fig. 5-3**a. The XRD patterns of MMS showed characteristic peaks at 2θ = 30.1º (220), 35.4º (311), 43.4º (400), 53.5º (422), 57.2º (511) and 62.6º (440), which confirmed the presence of magnetic Fe_3O_4 in the MMS nanoparticles (JCPDS:75-0033). In basic medium, the Fe(III) and Fe(II) ions as iron precursors will coprecipitate to form magnetite Fe_3O_4 nanoparticles. The broad peak at 25º indicated the amorphous phase of silica. The XRD pattern of MIL-100(Fe) is similar with the reported study and showed some characteristic peaks at 3.4º(220), 4.0º (311), 4.8º (400), 5.3º (331), 5.9º (422), and 6.3º(333).[5] The diffraction of both MMS and bare MIL-100(Fe) existed in the XRD patterns of MMS@MIL-100(Fe) composite, indicating the successful formation of MMS@MIL-100(Fe).

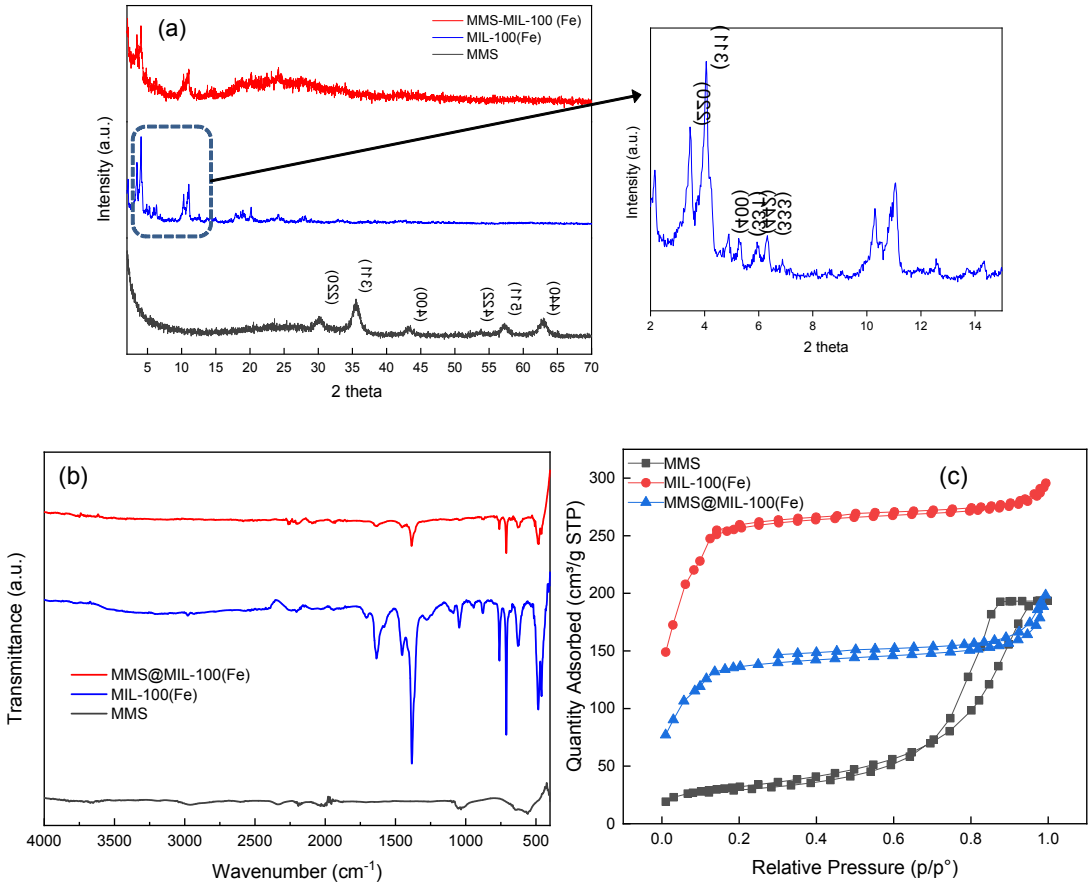

Fig. 5-3. XRD diffractograms (a); FTIR spectra (b); N_2 adsorption-desorption isotherms curve (c).

FTIR spectra of MMS, MIL-100(Fe) and MMS@MIL-100(Fe) are presented in **Fig. 5-3**b. An absorption band at 1046 cm^{-1} was attributed to the Si-O bonding vibration of SiO_2. This absorption band was observed in both FTIR spectra of MMS and MMS@MIL-100(Fe) composite. The absorption band at 1634 cm^{-1}, which corresponded to $–COO^-$ functional group, emerged in both spectra of bare MIL-100(Fe) and MMS@MIL-100(Fe) composite. These results suggested the successful synthesis of MMS@MIL-100(Fe) composite.

The N_2 gas adsorption-desorption isotherms of MIL-100(Fe) and MMS@MIL-100(Fe) composites at 77 K are given in **Fig.5-3**c. According to IUPAC classification, the N_2 adsorption-desorption isotherms curves of both MIL-100(Fe) and MMS@MIL-100(Fe) indicated the type-IV isotherm.[6] The BET surface area of the MMS@MIL-100(Fe) composite decreased by factor 2

compared to the pristine MIL-100(Fe) due to the incorporation of MMS nanoparticles. The physical properties of the synthesized materials are listed in **Table 5-1**.

Table 5-1. Physical properties of the adsorbents.

Adsorbent	BET surface area ($m^2 g^{-1}$)	Pore volume ($cm^3 g^{-1}$)	Average pore size (nm)
MIL-100(Fe)	915.0	0.451	1.97
MMS@MIL-100(Fe)	493.0	0.292	2.37

5.3.2 Adsorption of MB and CR

The effect of contact time on the adsorption of MB and CR onto MMS@MIL-100(Fe) composite is shown in **Fig. 5-4**. The adsorption of both dyes increased with the increase ofinteraction time until the equilibrium. At the initial stage, the composite adsorbent still had abundantly available adsorption sites, which could gradually increase the number of dyes adsorbed onto the composite. With the increase of time, the dye molecules had occupied the adsorption sites, causing the adsorption process to proceed at a slower rate until the equilibrium was reached. From **Fig. 5-4**, it can be seen that MMS@MIL-100(Fe) and pristine MIL-100(Fe) could adsorb MB dye better than CR dye.Since the molecular size of MB dye (1.7 nm)[7] was smaller than the average pore size of both pristine and composite MIL-100(Fe), the diffusion of MB molecule into the pore channels of the adsorbents was easier compared to that of the CR dye which has a bigger molecular size (2.3 nm).[8]

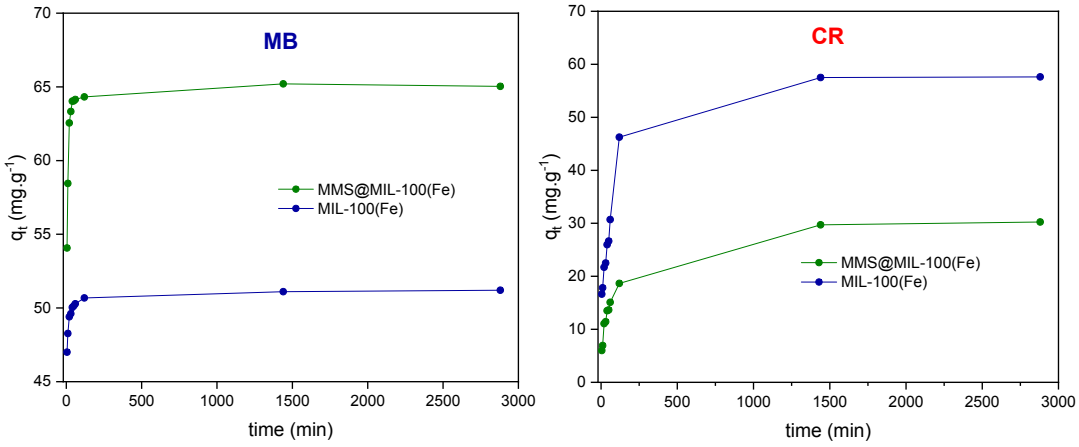

Fig. 5- 4. Adsorbed amount of MB and CR dyes onto the adsorbents over time.

To study the kinetics of MB and CR adsorption onto the composite, the experimental data were studied using pseudo-first and pseudo-second kinetic models and the kinetic parameters are summarized in **Table 5-2**. The higher correlation coefficient (R^2) of pseudo-second order model suggested that the adsorption of MB and CR onto the composite could be explained using the pseudo-second order kinetic model. Generally, the pseudo-second order model implies the chemisorption process and the dependency of the adsorption process on the amount of active sites and the amount of dyes adsorbed on the surface of the adsorbent.[9]

Table 5-2. The kinetic parameters of MB and CR adsorption.

Adsorbent	Dye	Pseudo-first order model			Pseudo-second order model		
		q_e (mg g^{-1})	k_1 (min^{-1})	R^2	q_e (mg g^{-1})	k_2 (g mg^{-1} min^{-1})	R^2
MIL-100(Fe)	MB	5.8	2.6x10^{-2}	0.531	50.9	3.2·10^{-2}	0.999
	CR	49.3	1.2x10^{-2}	0.946	29.1	5.8·10^{-3}	0.989
MMS@MIL-100(Fe)	MB	8.8	3.0x10^{-2}	0.558	64.8	1.9·10^{-2}	0.999
	CR	24.6	7.1x10^{-3}	0.871	17.8	4.3·10^{-3}	0.980

The adsorption isotherms of MB and CR dyes onto pristine MIL-100(Fe) and MMS@MIL-100(Fe) composite were studied using Langmuir and Freundlich isotherm models and the isotherm parameters of both models are given in **Table 5-3**. The higher R^2 values of

Langmuir isotherm model suggested that the adsorption of MB and CR dyes on each adsorbent was better explained by Langmuir isotherm model. The Langmuir isotherm model assumes the monolayer adsorption process on the homogeneous surface of pore channels.[10] Despite the lower BET surface area, the maximum adsorption capacity (q_{max}) of MMS@MIL-100(Fe) composite for MB dye was higher than that of the bare MIL-100(Fe).This suggested that the adsorption capacity of the composite in this study was not merely determined by the physical properties (i.e. porosity and surface area) of the adsorbent.[11] The electrostatic interaction between dyes and the adsorbent might also have an important role on the adsorption capacity. However, for anionic CR dye, the bare MIL-100(Fe) showed a higher adsorption capacity. This result suggested that the combination of MMS and MIL-100(Fe) to form MMS@MIL-100(Fe) composite could improve its adsorption ability for cationic dye, showing a potential for removing cationic dyes from real wastewater.

Table 5-3. The isotherm parameters of MB and CR adsorption.

Adsorbent	Dye	Langmuir isotherm			Freundlich isotherm		
		q_{max}(mg g^{-1})	K_L(L mg^{-1})	R^2	1/n	K_F (mg L^{-1})	R^2
MIL-100(Fe)	MB	209.2	0.821	0.987	0.435	82.5	0.825
	CR	91.7	1.278	0.951	0.172	45.4	0.680
MMS@MIL-100	MB	243.9	0.765	0.974	0.518	92.2	0.860
(Fe)	CR	47.3	0.211	0.980	0.249	17.8	0.858

5.4 Conclusions

In this study, magnetic mesoporous silica (MMS) and MIL-100(Fe) were incorporated to form MMS@MIL-100(Fe) composite and used in the adsorption of cationic MB and anionic CR dyes in water. The adsorption of both types of dyes onto the composite could be explained with pseudo-second order kinetic model and Langmuir isotherm model. Compared to the pristine MIL-100(Fe), the composite showed an enhanced adsorption capacity towards the cationic dye, showing its potential as an adsorbent for cationic dyes in water.

5.5 References

1. M. T. Yagub, T. K. Sen, S. Afroze, and H. M. Ang, *Adv. Coll. Interf. Sci.*, **2014**, 209, 172-184. https://doi.org/10.1016/j.cis.2014.04.002.
2. Y. Zhou, L. Yu, Y. Gao, J. Wu, and W. Dai, *Ind. Eng. Chem. Res.*, **2019**, 58, 19202-19210. https://doi.org/10.1021/acs.iecr.9b03815.
3. P. Kumar, A. Pournara, K. Kim, V. Bansal, S. Rapti, and M. J. Manos, *Prog. Mater. Sci.*, **2017**, 86, 25-74. https://doi.org/10.1016/j.pmatsci.2017.01.002.
4. M. Tong, D. Liu, Q. Yang, S. Devautour-Vinot, G. Maurin, and C. Zhong, *J. Mater. Chem. A,***2013**, 1, 8534-8537. https://doi.org/10.1039/C3TA11807J.
5. Z. Kozakova, I. Kuritka, N. E. Kazantseva, V. Babayan, M. Pastroek, M. Machovsky, P. Bazant, and P. Saha, *Dalton Trans.,* **2015**, 44, 21099-21108. https://doi.org/10.1039/C5DT03518J.
6. M. Thommes, K. Kaneko, A. V. Neimark, J. P. Olivier, J. P.; F. Rodriguez-Reinoso, J. Rouquerol, and K. S. W. Sing, *Pure Appl. Chem.*, **2015**, 87, 1051-1069. https://doi.org/10.1515/pac-2014-1117.
7. L. Li, X. L. Liu, M. Gao, W. Hong, G. Z. Liu, L. Fan, B. Hu, Q. H. Xia, L. Liu, G. W. Song, and Z. S. Xu, *J. Mater. Chem. A*, **2014**, 2, 1795-1801. https://doi.org/10.1039/C3TA14225F.
8. Q. Wu, H. Liang, M. Li, B. Liu, and Z. Xu, *Chinese J. Polym. Sci.*, **2016**, 34, 23-33. https://doi.org/10.1007/s10118-016-1723-6.
9. S. Lin, Z. Song, G. Che, A. Ren, P. Li, C. Liu, and J. Zhang, *Micropor. Mesopor. Mat.,* **2014**, 193, 27-34. https://doi.org/10.1016/j.micromeso.2014.03.004.
10. X. Guo, S. Han, J. Yang, X. Wang, S. Chen, and S. Quan, *Ind. Eng. Chem. Res.*, **2020**, 59, 2113-2122. https://doi.org/10.1021/acs.iecr.9b05715.
11. A. C. Tella, J. T. Bamgbose, V. O. Adimula, M. Omotoso,S. E. Elaigwu, V. T. Olayemi, and O. A. Odunola, *SN Appl. Sci.*, **2021**, 3(136). https://doi.org/10.1007/s42452-021-04163-w.

Chapter 6

General conclusions and future perspectives

6.1 General conclusions

This study focused on the development of magnetic mesoporous silica-based composite for the removal of synthetic dyes from water. The synthesis methods used in this study are the more environmentally friendly methods such as one-pot synthesis method and microwave-assisted method.

Magnetic mesoporous silica (MMS) composites were synthesized in a one-pot system using various alkanolamines as a basic catalyst. The synthesized MMS were characterized thoroughly to understand the characteristics of the MMS. MMS composites showed excellent capacity in removing brilliant green dye from solution. In addition, the MMS composites showed a fast adsorption kinetics and good recyclability.

The composite Fe_3O_4@SiO_2 (core shell) and a type of metal organic frameworks, MIL-100(Fe),has been synthesized under microwave irradiation. The synthesizedFe_3O_4@SiO_2-MIL-100(Fe) composite showed high selectivity for Congo red (CR) dye and showed an enhanced adsorption capacity compared to the pristine MIL-100(Fe). In addition, the used composite could be easily separated using an external magnetic force. These results showed the potential of the composite as a superior adsorbent for CR dye.

Although the magnetic mesoporous silica-based composites synthesized in this study showed superior performance in dye adsorption process, the application of the composite in a scale-up process is still questionable. Many aspects related to the optimization of the synthesis and adsorption processes are still needed.

6.2 Future perspectives

- The composites in this study showed excellent performance in the adsorption of dyes from water. The investigation on the ability of the composites to remove other types of water contaminants such as heavy metals, anions, pharmaceuticals, etc. is worth conducting.
- The removal of dyes in this study were conducted in a batch system. The use of a batch system limited the use of composites for practical applications. Further studies in the removal of dyes in a fixed-bed column test can be carried out to investigate the potential use of the composites for industrial purpose. In order to be applied in a column test, composite adsorbents with a larger particle size are needed.
- Since this study is obtained through empirical studies, a more in-depth theoretical simulations could be beneficial to further understand the composite and their behaviors.

List of figures

Fig. 2-1. Adsorption process 6

Fig. 2-2. Possible mechanism of mesostructure formation in MCM-41 9

Fig. 2-3. Schematic representation of the synthesis of MIL-100(Fe) 10

Fig. 3-1. Molecular structure of brilliant green dye 16

Fig. 3-2. One-pot synthesis of magnetic mesoporous silica 17

Fig. 3-3. Molecular structure of alkanolamines: triethanolamine (a); diethanolamine (b); tris(hydroxymethyl)aminomethane (c) 18

Fig. 3-4.TEM (a); SEM images and EDX spectra (b) of MMS 20

Fig. 3-5. XRD diffractogram (a); FTIR spectra (b); Nitrogen adsorption-desorption isotherm (c) of MMS composites 21

Fig. 3-6. XPS spectra of MMS before (a) and after (b) adsorption of BG 24

Fig.3-7. Effect of initial pH on adsorption and concentration of BG 25

Fig. 3-8. Pseudo-first order kinetic (a) and Pseudo-second order kinetic (b) models of BG onto MMS composites 27

Fig. 3-9. Adsorption isotherms of BG onto MMS composites 28

Fig. 3-10. Proposed adsorption mechanism of brilliant green onto MMS 30

Fig. 3-11. Recyclability of MMS composites as adsorbents for BG 31

Fig. 4-1. Microwave-assisted synthesis of magnetic Fe_3O_4@SiO_2-MIL-100(Fe) composite 38

Fig. 4-2. SEM images of Fe_3O4@SiO_2 nanoparticles (a); MIL-100(Fe) (b); Fe_3O_4@SiO_2-MIL-100(Fe) (c); TEM images of MIL-100(Fe) (d); Fe_3O_4@SiO_2-MIL-100(Fe) (e) 43

Fig. 4-3. XRD diffractogram (a); FTIR spectra (b); N_2 adsorption-desorption isotherm (c); and TGA curve (d) of the adsorbents 43

Fig. 4-4. Various dye solution before and after addition of Fe_3O_4@SiO_2-MIL-100(Fe) (a); UV-visible spectra of dyes before and after adsorption process (b) 46

Fig. 4-5. Pseudo-first order (a); pseudo-second order (b); and intra-particle diffusion (c) kinetic models 47

Fig. 4-6. Adsorption isotherm parameter plots for MIL-100(Fe) (a) and Fe_3O_4@SiO_2-MIL-100(Fe) (b) 50

Fig. 4-7. Mechanism of CR adsorption onto Fe_3O_4@SiO_2-MIL-100(Fe) composite 51

Fig. 4-8. Bar graph of the recyclability of Fe_3O_4@SiO_2-MIL-100(Fe) 52

Fig. 5-1. Schematic diagram of the synthesis of MMS@MIL-100(Fe) 58

Fig. 5-2. SEM images of MIL-100(Fe) (a) and MMS@MIL-100(Fe) (b); TEM images of MIL-100(Fe) (c) and MMS@MIL-100(Fe) (d) 60

Fig. 5-3. XRD diffractograms (a); FTIR spectra (b); N2 adsorption-desorption isotherms curve (c) 61

Fig. 5- 4. Adsorbed amount of MB and CR dyes onto the adsorbents over time 63

List of tables

Table 3-1. Result of EDX measurement 20

Table 3-2. Textural properties of MMS composites 23

Table 3-3. Adsorption kinetic parameters of BG onto MMS composites 26

Table 3-4. Adsorption isotherm parameters of BG onto MMS composites 28

Table 3-5. Comparison of the maximum adsorption capacity of various adsorbents towards BG dye 29

Table 4-1. Chemical structure of various organic dyes in this study 40

Table 4-2. Physical properties of MIL-100(Fe) and Fe3O4@SiO2-MIL-100(Fe) 45

Table 4-3. Kinetic parameters of CR adsorption onto the prepared adsorbents 48

Table 4-4. Isotherm parameters of CR adsorption onto the adsorbents 49

Table 4-5.Comparison maximum adsorption capacity of various magnetic adsorbents for CR dye 50

Table 5-1. Physical properties of the adsorbents 62

Table 5-2. The kinetic parameters of MB and CR adsorption 63

Table 5-3. The isotherm parameters of MB and CR adsorption 64

List of publications

1. One-pot alkanolamines-assisted synthesis of magnetic mesoporous silica for synthetic dye adsorption. (Analytical Sciences, accepted)

2. Preparation and characterization of magnetic mesoporous silica@MIL-100(Fe) composite for the removal of cationic and anionic dyes from water. (Journal of Engineering Science and Technology, accepted)

List of presentations

1. The 10th Forum on Studies of Environmental and Public Health Issues in Asian Mega-cities (EPAM), Gifu University, Gifu, Japan, December 11-15, 2019 (Poster presentation).

2. The 32nd Conference of the Society for Chromatographic Sciences, Tokyo University of Science, Noda, Japan, November 25-27, 2021 (Poster presentation).

3. The 3rd International Seminar on Science and Technology (ISSTEC), Yogyakarta, Indonesia, November 30, 2021 (Poster presentation).

Curriculum vitae

Puji Lestari

Born on October 20, 1987 in Mataram, West Nusa Tenggara, Indonesia.

Married to Gani Purwiandono

Mother of Raffaza Abdullah and Aqila Khairunnisa

Education

2003-2006 : Senior High School No. 1 Mataram, Indonesia.

2006-2010 : Bachelor program at Chemistry Department of Universitas Gadjah Mada, Yogyakarta, Indonesia.

2011-2014 : Dual Degree Master Program between Chemistry Department of Universitas Gadjah Mada, Indonesia (1 year) and Institute of Environmental and Sustainable Chemistry of Technische Universität Braunschweig, Germany (2 years).

2019-2022 : Doctoral Program at Engineering Division, Graduate School of Engineering, Gifu University, Japan.

Professional Experience

2015 – present : Staff of Environmental Engineering Department, Universitas Islam Indonesia, Yogyakarta, Indonesia.

Acknowledgement

In the name of Allah, the All-Merciful and the Most Compassionate. Praise be to Allah, the Lord of all the universe(s).

I would like to express my gratitude to **Prof. Lee Wah Lim** for the continuous support, help, and kindness during my study and life in Japan. She is the best supervisor every student could ask for. My sincere gratitude to **Prof. Toyohide Takeuchi** for giving me the opportunity to become the member of his lab.

I am thankful to **Advance Global Program (AGP)** in Graduate School of Engineering, Gifu University and **Universitas Islam Indonesia** for the financial support of my doctoral study.

I would like to thank **Prof. Yutaka Ohya** and **Prof. Fusheng Li** for their helpful comments and suggestions.

I am grateful for the unconditional love and support from my mother **Husniah** and my deceased father, **Guna Abadi**, who passed away last June. I would not be where I am today without both of them.

Finally, I would like to acknowledge the most important persons in my life – my husband **Gani Purwiandono**, my son **Raffaza Abdullah**, and my daughter **Aqila Khairunnisa**. They have been the source of my strength throughout this journey.

Puji L.

March 2022